UCRL-11004 Rev.
c.2

University of California

Ernest O. Lawrence Radiation Laboratory

TWO-WEEK LOAN COPY

This is a Library Circulating Copy which may be borrowed for two weeks. For a personal retention copy, call Tech. Info. Division, Ext. 5545

Berkeley, California

UCRL-11004 Rev.
c.2

DISCLAIMER

This document was prepared as an account of work sponsored by the United States Government. While this document is believed to contain correct information, neither the United States Government nor any agency thereof, nor the Regents of the University of California, nor any of their employees, makes any warranty, express or implied, or assumes any legal responsibility for the accuracy, completeness, or usefulness of any information, apparatus, product, or process disclosed, or represents that its use would not infringe privately owned rights. Reference herein to any specific commercial product, process, or service by its trade name, trademark, manufacturer, or otherwise, does not necessarily constitute or imply its endorsement, recommendation, or favoring by the United States Government or any agency thereof, or the Regents of the University of California. The views and opinions of authors expressed herein do not necessarily state or reflect those of the United States Government or any agency thereof or the Regents of the University of California.

UCRL-11004 (Rev)

UNIVERSITY OF CALIFORNIA

Lawrence Radiation Laboratory
Berkeley, California

AEC Contract No. W-7405-eng-48

MEASUREMENTS OF THE MUON-CAPTURE RATE IN He^3 AND He^4

Leonard B. Auerbach, Robert J. Esterling, Roger E. Hill,
David A. Jenkins, Joseph T. Lach, and Norman H. Lipman

October 8, 1964

Measurements of the Muon-Capture Rate in He^3 and He^4 †

Leonard B. Auerbach,* Robert J. Esterling,* Roger E. Hill,*
David A. Jenkins, Joseph T. Lach,* and Norman H. Lipman*

Lawrence Radiation Laboratory
University of California
Berkeley, California

October 8, 1964

ABSTRACT

In order to test the universality of the V-A Fermi interaction and the presence of the induced pseudoscalar term in the Hamiltonian, we have measured the rate of the reaction $\mu^- + He^3 \rightarrow H^3 + \nu_\mu$. This reaction is closely analogous to the fundamental muon-capture interaction $\mu^- + p \rightarrow n + \nu_\mu$. We have also measured the total muon-capture rates in He^3 and He^4; that is, the rates for the reactions $\mu^- + He^3 \rightarrow$ all final states and $\mu^- + He^4 \rightarrow$ all final states. Negative muons were brought to rest in a high-pressure helium-gas target. The capture processes all yield a charged particle whose energy was measured by observation of scintillation in the helium gas. Captures into the H^3 channel were recognized by the unique energy (1.9 MeV) of the triton recoil. The total capture rates obtained were: $\Lambda(He^3) = 2170 \pm^{170}_{430}\ sec^{-1}$, and $\Lambda(He^4) = 375 \pm^{30}_{300}\ sec^{-1}$. The partial capture rate to the triton ground state was measured as $\Lambda(He^3 \rightarrow H^3) = 1505 \pm 46\ sec^{-1}$. These results are in good agreement with theoretical predictions based on a universal Fermi interaction, and on a conserved vector current. They also indicate a positive-induced-pseudoscalar-coupling coefficient, but interpretation of these results in terms of the fundamental muon-capture process is somewhat ambiguous because of the uncertainty in the structure of the helium nucleus.

I. INTRODUCTION

When a negative muon comes to rest in matter it goes into a Bohr orbit with $n, \ell \approx 15$, from which it cascades down by x-ray and Auger processes to the 1s atomic state in $\approx 10^{-10}$ sec.[1] When the muon reaches the ground state it either decays according to

$$\mu^- \rightarrow e^- + \nu_\mu + \bar{\nu}_e \tag{1}$$

or it interacts with the nucleus according to the basic reaction,[2]

$$\mu^- + p \rightarrow n + \nu_\mu \, . \tag{2}$$

We call this nuclear interaction "muon capture."[3]

When a negative muon is captured by a He^3 nucleus, three principal reactions occur:

$$\mu^- + He^3 \rightarrow H^3 + \nu_\mu \tag{3}$$

$$\mu^- + He^3 \rightarrow H^2 + n + \nu_\mu \tag{4}$$

$$\mu^- + He^3 \rightarrow H^1 + n + n + \nu_\mu \, . \tag{5}$$

Since there are no known excited states of the triton (H^3) nucleus, reaction (3) presumably goes directly to the ground state of the triton. The isodoublet (He^3, H^3) with spin 1/2, called the "trion," is analogous to the proton-neutron doublet, and Eq. (3) closely resembles the basic muon-capture reaction (2). Since reaction (3) has a two-body final state, energy and momentum conservation show that the triton will recoil with a unique energy (1.8959 ± 0.0001 MeV). Our experiment is designed primarily to measure Λ_C, the partial capture rate to the triton ground state, by observation of this monoenergetic recoil.

Reactions (4) and (5) represent muon captures that result in an unbound triton and are referred to as the breakup reactions in this paper. These breakup reactions involve three- and four-body final states with the charged-particle momentum ranging from 0 to about 350 MeV/c. The breakup events constitute a background to the measurement of the $He^3 \rightarrow H^3$ events. The breakup capture rate Λ_B is also measured in this experiment, although with much less accuracy than is Λ_C. The theoretical analysis of the breakup reactions is not so clearcut as with reaction (3); however, Yano[4] has recently completed a detailed analysis of reaction (4). It is interesting to compare the probability of capture from the same nucleus into various channels because one can test the coupling coefficients and the nuclear-wave function better when several channels are involved than when there is only one final state.

To determine Λ_C we measured the ratio of stopped muons giving a triton recoil (T) to the total number of stopped muons (Sμ). The capture rate is computed from the proportionality

$$\Lambda_C/\Lambda_T = T/S\mu \tag{6}$$

where the total muon-disappearance rate is $\Lambda_T = \Lambda_B + \Lambda_C + \Lambda_D$ and the muon-decay rate is[5] $\Lambda_D = 1/(2.200 \pm 0.002\ \mu\text{sec}) = 4.545 \times 10^5\ \text{sec}^{-1}$.

Similarly the breakup capture rate is

$$\Lambda_B = (B/S\mu)\Lambda_T, \tag{7}$$

where B is the number of observed breakup events. Only about 1 muon in 300 is captured to the triton ground state, and about 1 in 600 is captured to the breakup states. The remainder decay according to reaction (1). One of the experimental problems is to distinguish the decay electron from the relatively rare capture events.

Most of the experimental tests were performed with He^4 before He^3 was put in the target. Consequently a measurement of the muon-capture rate in He^4 was made concomitant with the He^3 measurement. The principal reaction in He^4,

$$\mu^- + He^4 \rightarrow H^3 + n + \nu, \tag{8}$$

is very similar to the breakup reaction (4), and the experimental analysis is very similar to the analysis of the breakup reactions.

Previous measurements and theoretical predictions of the muon-capture rates are listed in Table I. Our experiment is an attempt to make a more precise measurement of Λ_C by the use of helium scintillation. A preliminary account of the $He^3 \rightarrow H^3$ capture-rate measurement was reported previously;[6] the experiment is described and analyzed in greater detail in this article.[7] The slight shift in the value of Λ_C reflects a more careful analysis of the corrections.

II. THEORY

The main emphasis of this theoretical discussion is on the calculation of the transition rate of Eq. (3), since the main purpose of the experiment described here is to measure that rate.

A. The Interaction Hamiltonian

The interaction Hamiltonian responsible for μ decay is[25]

$$\mathcal{H} = \frac{G}{\sqrt{2}} [\bar{u}(e)\,(1 - \gamma_5)\gamma_\lambda\, u(\nu_e)][\bar{u}(\nu_\mu)\,(1 - \gamma_5)\gamma_\lambda\, u(\mu)] + \text{H.C.} \tag{9}$$

Here H.C. means the Hermitian conjugate, the u's are Dirac spinors, and the γ's are the Dirac matrices. The weak-interaction coupling constant G, evaluated from decay rate of the positive muon, is[14]

$$G = 1.0263 \pm 0.0004 \times 10^{-5}/m_p^2 \approx 1.43 \times 10^{-49} \text{ erg-cm}^3, \qquad (10)$$

where m_p is the proton mass. The basic postulate of the universal Fermi interaction (UFI) viewpoint is that the same Hamiltonian and the same coupling constant G describe the weak interaction between any four fermions. One has just to replace μ, e, ν_μ, and ν_e by the relevant particles. Unfortunately, except for muon decay and neutrino scattering, strong interactions come into play in every weak interaction and virtual pion effects must be expected to alter the effective interaction. In the particular case of nuclear β decay, the interaction is modified to an effective Hamiltonian

$$\mathcal{H} = \frac{G}{\sqrt{2}} \left[\bar{u}(e)\,(1 - \gamma_5)\gamma_\lambda\, u(\nu_e)\right] \left[\bar{u}(p)\,(V_\beta + A_\beta\gamma_5)\gamma_\lambda\, u(n)\right] + \text{H. C.} \qquad (11)$$

where $V_\beta \approx 1.0$ and $A_\beta \approx -1.2$ are the vector and axial-vector coupling coefficients that take strong interactions into account. This β-decay interaction [Eq. (11)] is sufficient to describe the situation in the limit of zero-momentum transfer. In muon capture, however, the momentum transfer is ≈ 100 MeV/c and this further modifies the Hamiltonian. The Hamiltonian that is effective in muon capture was first presented by Goldberger and Treiman[26] but later modified by Weinberg[27] to the form:

$$\mathcal{H} = \frac{G}{\sqrt{2}} \left[\bar{u}(n) \left(V\gamma_\lambda + A\gamma_5\gamma_\lambda + M\sigma_{\lambda a}\frac{q_a}{m_p} + T\sigma_{\lambda a}\gamma_5\frac{q_a}{m_p} + S\frac{q_\lambda}{m_p} + P\gamma_5\frac{q_\lambda}{m_p}\right) u(p)\right] \left[\bar{u}(\nu_\mu)\,(1 - \gamma_5)\gamma_\lambda\, u(\mu)\right] + \text{H. C.} \qquad (12)$$

This is the most general interaction Hamiltonian that (a) is Lorentz invariant, (b) has no derivatives in the leptonic fields, (c) reduces to Eq. (9) in the absence of strong interactions, and (d) reduces to Eq. (11) in the presence of strong interactions at zero-momentum transfer. In

this Hamiltonian, $q_\alpha = p_\alpha - n_\alpha = \nu_\alpha - \mu_\alpha$ is the four-momentum transfer; $\sigma_{\alpha\beta} = 1/2(\gamma_\alpha\gamma_\beta - \gamma_\beta\gamma_\alpha)$; and V, A, M, T, S, and P are the coupling coefficients of the vector, the axial-vector, the weak magnetism, the tensor, the induced scalar, and the induced pseudoscalar terms, respectively. These coupling coefficients are dimensionless functions of q^2 and can all be chosen real if the interaction is time-reversal-invariant.

B. Coupling Coefficients

In this section, we evaluate the coupling coefficients of Eq. (12) so far as is possible with present theories. The trion is treated both as a single Dirac particle[14,28] (with all nuclear-structure effects absorbed into the coupling coefficients) and as a composite of nucleons.[16]

1. Vector and "Weak Magnetism" Coefficients

The vector V and weak-magnetism M coefficients in the Hamiltonian (12) are the only coefficients that can be determined with some degree of confidence. This is because the conserved-vector-current (CVC) theory[29] seems to be valid in nuclear and pion-beta decay,[30] and thus should also apply in muon capture. The coefficients V and M can then be related directly to the electric and magnetic isovector form factors measured in electron scattering. If He^3 and H^3 electron scattering is used,[31] one obtains for the trion[14,28]

$$\begin{aligned} V(q^2 = 0.27\ F^{-2}) &= 0.80 \pm 0.10 \\ M(q^2 = 0.27\ F^{-2}) &= -2.39 \pm 0.10. \end{aligned} \quad \text{(trion)} \qquad (13)$$

On the other hand, electron-nucleon scattering gives[32]

$$V(q^2 = 0.25\ F^{-2}) = 0.97 \qquad \text{(nucleon)} \qquad (14)$$
$$M(q^2 = 0.25\ F^{-2}) = 1.797.$$

Note that the sign of $M(q^2)$ for the nucleon is opposite that for the trion. One way to understand this opposite sign is by considering He^3 and H^3 as a closed-shell nucleus, He^4, minus a neutron or a proton.[33] The missing particle (hole) gives He^3 and H^3 the properties of an antineutron and antiproton, respectively. Since the magnetic moments of the antinucleons are opposite in sign from those of the nucleons, the weak-magnetism coefficient must also have opposite sign.

2. Axial-Vector Coefficient

The axial-vector coefficient at zero-momentum transfer A(0) can be found from the ft value of tritium:[25,34]

$$ft = \frac{2\pi^3 \ln 2}{(Gm_p^2)^2[V_\beta^2(0) + 3\,A_\beta^2(0)]} \left(\frac{m_p}{m_e}\right)^4 \frac{\hbar}{m_e c^2} = 1132 \pm 40 \text{ sec.} \qquad (15)$$

By the hypothesis of the CVC theory, $V_\beta(0) = 1.0$ and one may solve for $|A_\beta(0)| = 1.194 \pm 0.037$. By the principles of UFI, $A_\beta(0)$ in beta decay is the same coefficient as that in muon capture. Therefore for the trion we have

$$|A(0)| = 1.194 \pm 0.037. \qquad \text{(trion)} \qquad (16)$$

Similar analysis using the ft value of the neutron gives

$$|A(0)| = 1.20 \pm 0.04. \qquad \text{(nucleon)} \qquad (17)$$

The experiments on muon capture in hydrogen[2] have established that for the nucleon the sign of A is opposite to that of V, i.e., we have a V-A theory. For the trion, A must have the sign opposite to that of the A of the nucleon, again because of the correspondence $He^3 \longleftrightarrow He^4 + \bar{n}$ and

$H^3 \leftrightarrow He^4 + \beta$. Therefore since $A(0) = +1.20$ for the nucleon, $A(0) = +1.194$ for the trion.

There is no proven theory or experimental information for the dependence of A on q^2 in the case of the trion. One can hypothesize that, since the axial-vector term and the weak-magnetism term in the Hamiltonian reduce to the same form in the nonrelativistic limit, $A(q^2)/A(0) = M(q^2)/M(0)$. An alternative choice is that this ratio is equal to $V(q^2)/V(0)$. In the case of the nucleon a dispersion-theoretical argument indicates that[16]

$$\frac{A(q^2)}{A(0)} \approx 1 - \frac{q^2}{4\pi m_p^2} = 0.999. \qquad (18)$$

However, because of nuclear-structure effects, the momentum dependence of A of the trion should be greater than that given in Eq. (18), and A is expected to be within ≈ 10% of +1.0.

3. Induced-Pseudoscalar Coefficient

Even less is known about the value of the induced pseudoscalar coefficient $P(q^2)$ than is known about $A(q^2)$. Dispersion-theoretical arguments,[26] which use the one-pion-exchange model, give for the nucleon[5]

$$g_P = \frac{m_\mu}{m_p} P(q^2) = \frac{2m_\mu m_p}{q^2 + m_\pi^2} A(0) = 6.6\, A(0) = -7.9 \quad \text{(nucleon)} \qquad (19)$$

For the trion, the proton mass must be replaced by the trion mass m_t and one obtains

$$\frac{m_\mu P(q^2)}{m_p} = \frac{2m_\mu m_t}{q^2 + m_\pi^2} A(0) = 19.7\, A(0) = +23.5. \quad \text{(trion)} \qquad (20)$$

An additional correction for many-body effects is probably also necessary for $P(q^2)$ of the trion, but since the dispersion argument is so uncertain this additional factor of 0.8 to 0.9 has been neglected. Measurements of the angular distribution of neutrons from muon capture in calcium[35] and

measurements[36] of muon capture in O^{16} populating discrete levels of N^{16} yield values of g_P/A (nucleon) between 5 and 30, depending on the experiment and its interpretation. Most measurements are consistent with this ratio close to 10.

4. Induced-Scalar and Tensor Coefficients

Nothing is known about the values or the signs of the S and T coefficients of Eq. (12). These are the "second class" terms which, as Weinberg pointed out,[27] could also be present in the Hamiltonian. Most authors assume that the weak currents have a definite G-conjugation parity (that of the V and A terms) and that therefore $S = T = 0$. If S and T are not zero, these second-class terms could radically affect the capture rate in both hydrogen and helium.

C. Hyperfine Effect

After a negative muon comes to rest in matter, the atomic system consisting of the muon and the nucleus is initially formed in a statistical mixture of $I \pm 1/2$ spin states (I is the spin of the nucleus). These two angular-momentum states are called hyperfine states, because they are analogous to hyperfine states in a normal atom. For an $I = 1/2$ nucleus, and with only V and A coupling in Eq. (12), the hyperfine singlet- and triplet-capture rates reduce in the nonrelativistic limit to

$$\Lambda_s \propto |V - 3A|^2 \text{ and } \Lambda_t \propto |V + A|^2. \tag{21}$$

Thus if the coefficient $V \approx -A$ (as in muon capture in hydrogen), $\Lambda_t \approx 0$. In the case of capture in He^3, $V \approx +A$ (see Sec. II. B), and the two hyperfine rates are approximately equal. Detailed calculations give[37]

$\Lambda_s = 713\ sec^{-1}$ and $\Lambda_t = 16.9\ sec^{-1}$ in hydrogen and $\Lambda_s = 1806\ sec^{-1}$ and $\Lambda_t = 1312\ sec^{-1}$ for muon capture in He^3. This spin dependence makes it important to know the relative populations of singlet and triplet states at time of capture.

Winston and Telegdi[38] have investigated hyperfine transitions in muonic atoms both theoretically and experimentally. They find that in the lighter elements transitions take place by internal conversion (electron ejection) at rates comparable to the muon's lifetime. However, in He^3 the hyperfine splitting is $\approx$ 1.4 eV, and this is not enough energy to eject the single K electron that may surround the μ-He^3 atomic system. Thus, if internal conversion is the major cause of hyperfine transitions, there should be no transitions between the hyperfine levels in He^3 during the muon's lifetime and the hyperfine states should have just their original statistical population. It should be emphasized that this is not the case in hydrogen, for which exchange collisions provide the mechanism for hyperfine transitions (see Appendix).

D. $He^3 \rightarrow H^3$ Capture Rate - Method I

This method of calculating Λ_C, the capture rate of reaction (3), was recently proposed by Fujii and Yamaguchi[14] and independently by Drechsler and Stech.[28] In this calculation the free trion is assumed to satisfy the Dirac equation and the nucleon spinors of Eq. (12) are replaced by trion spinors. All the nuclear-structure effects are absorbed into the coupling coefficients analogously to the way nucleon structure is absorbed into the electromagnetic form factors in electron-nucleon scattering. Thus the calculation is completely relativistic and is as accurate as the single-proton calculation. The difficulties that remain are (a) to fix the coupling coefficients for the trion and (b) to interpret the trion results in terms of single-proton capture.

The capture rate can be obtained directly from the calculation of Adams for proton capture.[37] One has merely to interpret his results for the singlet- and triplet-capture rates in terms of the trion. If the following coupling coefficients (Sec. II. B)

$$V = 0.80 \qquad M = -2.39 \qquad S = 0$$
$$A = 1.00 \qquad P = 208.7 \qquad T = 0 \tag{22}$$

are used to calculate the capture rates, one then obtains $\Lambda_s = 1806\ \mathrm{sec}^{-1}$ and $\Lambda_t = 1312\ \mathrm{sec}^{-1}$, which combine to give $\Lambda_C = 1/4\ \Lambda_s + 3/4\ \Lambda_t = 1435\ \mathrm{sec}^{-1}$ for a statistical population. If each coupling coefficient is varied one at a time from the values given in Eq. (22), the effect on the capture rate is shown in Fig. 1. Note that Λ_C is not especially sensitive to V but is over three times more sensitive to A. Also note that Λ_s is especially sensitive to small changes in P. It would be interesting to induce transitions between the hyperfine levels in He^3, for, if a measurement of the $He^3 \rightarrow H^3$ capture rate from the hyperfine singlet state were possible, P could be determined rather accurately.

E. $He^3 \rightarrow H^3$ Capture Rate - Method II

This section outlines the method of calculating the $He^3 \rightarrow H^3$ capture rate given by Fujii and Primakoff.[16] The essential feature of this method is that the ratio of the nuclear-matrix element for muon capture and for tritium-beta decay is used to eliminate some of the uncertainty due to nuclear structure. The calculation is nonrelativistic, treats the trion as an aggregate of three nucleons, and does not include the S and T terms of the Hamiltonian [Eq. (12)].

The first step is to calculate the capture rate Λ_C in terms of the nuclear-matrix element expressed as a sum over the three nucleons in He^3.

The second step is to calculate the triton-beta-decay-transition rate, in which the roles of the He^3 and H^3 nuclei are interchanged. The third step is to form the ratio of the two transition rates. For this ratio one obtains

$$\frac{\Lambda_C}{\lambda_\beta} = \pi p_\nu^2 \left(1 - \frac{p_\nu}{m_\mu + m_{He}}\right) \frac{(Z\alpha m_\mu)^3}{f m_e^5} \frac{|M^\mu_{nucl}(He^3 \to H^3)|^2}{|M^\beta_{nucl}(H^3 \to He^3)|^2}, \tag{23}$$

$$= 3.05 \times 10^6 \times R,$$

where R is the ratio of the nuclear-matrix elements. The problem now is to evaluate R. Fujii and Primakoff obtain the following formula

$$R \approx \left(1 + \frac{x}{15}\right)^{-5} \left[1 - \frac{2\alpha Z m'_\mu}{p_\nu} \left(\frac{3x}{4}\right)^{1/2} \left(\frac{1-5x/18}{1-x/6}\right)\right] \left[\frac{G_V^2 + 3\Gamma_A^2}{G^2(V_\beta^2 + 3A_\beta^2)}\right] \tag{24}$$

where

$$\begin{aligned} G_V/G &= V(1 + p_\nu/2m_p), \\ \Gamma_A^2 &= G_A^2 + 1/3(G_P^2 - 2G_P G_A), \\ G_A/G &= A - V[1 + 1.79 - (-1.91)]\, p_\nu/2m_p, \\ G_P/G &= \left(\frac{m_\mu}{m_p} P - A - V[1 + 1.79 - (-1.91)]\right) p_\nu/2m_p, \\ x &= p_\nu^2 \langle r^2 \rangle; \\ \langle r^2 \rangle &= \int r^2 \rho(r)\, d^3r \end{aligned} \tag{25}$$

is the mean-square radius, and $\rho(r)$ is some density distribution of protons in the He^3 nucleus. The ratio R is close to unity and relatively independent of the nuclear model, but the interpretation of $\langle r^2 \rangle$ (or alternatively of ρ) is ambiguous. In electron-scattering experiments, Collard et al.[31] obtained 1.97 F for the charge radius of He^3 and 1.69 F for the magnetic-moment radius. This ambiguity in the nuclear radius is related to the uncertainty of $A(q^2)$ for the trion.

If one uses $\langle r^2 \rangle = (1.83F)^2$ (Fujii and Primakoff use 1.78F) and the values of G_V and Γ_A given by the coupling coefficients of the nucleon,

$$V = 0.97 \qquad \frac{m_\mu P}{m_p} = -7.9 \qquad V_\beta = 1.0$$
$$A = -1.2 \qquad A_\beta = -1.2 \tag{26}$$

one obtains $R \approx 0.808$. This value, together with $ft = 1132 \pm 40$ sec [32] and Eq. (23), yields

$$\Lambda_C = 3.05 \times 10^6 \ln(2) R/ft = 1518 \text{ sec}^{-1}. \tag{27}$$

Several authors have calculated the $He^3 \rightarrow H^3$ capture rate, but they differ in the choice of a wave function used to evaluate R, in the choice of the coupling coefficients, or in the value of the nuclear radius. Figure 2 shows the dependence of Λ_C on the nuclear radius and on the various coupling coefficients.

III. DESCRIPTION OF THE EXPERIMENT

The main purpose of the experiment is to measure $\Lambda_C = \Lambda_T T/S\mu$. To show how this is done, we first outline the experimental method used in determining the number of stopped muons, $S\mu$, and the number of triton recoils, T.

A. General Technique

Figure 3 is a rough schematic diagram of the system. A beam of negatively charged particles, extracted from the cyclotron, was momentum analyzed and focused on the helium target. The muon component of the beam was identified by a time-of-flight coincidence ($B\mu$) and by range. The helium gas served three purposes: (a) as a target for the muon-capture process,

(b) as a scintillation detector for muons that came to rest in the gas, and (c) as an energy spectrometer for measuring the energy of delayed events. A cup-shaped plastic scintillation counter (5) enclosed the gas, leaving only the beam-entrance direction free, and signaled muons that passed through the gas without stopping. Thus a stopped muon (Sμ) was identified electronically by a prompt coincidence of Bμ and the He counter (4) with an anticoincidence signal (veto) from the cup counter (5), i.e., $S\mu = B\mu\, He\, \bar{5}$. Delayed pulses from the He counter, occurring in the interval 0.2 to 6.4 μsec after Sμ, triggered the coincidence circuit TR and were then sorted on the basis of pulse height and timing. Counters 3 and 5, which surround the gas, were used to detect $\mu \rightarrow e$ decays, and any TR event that was associated with a pulse in counter 3 or 5 was vetoed. True triton recoils have a range of only 1.7 mm (at 28.9 atm) in the gas and were not vetoed. Thus, a TR event is of the type $TR = S\mu$ (delayed He $\bar{3}\,\bar{5}$). Such events opened a gate and allowed the He pulse height to be measured on a pulse-height analyzer (PHA). The resulting energy spectrum and the number of counts Sμ form the basic data.

Since a determination of the capture rate depends on how well we can distinguish the 1.9-MeV triton recoils from background events, an important part of the experiment was to make the helium scintillation process as efficient as possible. The results of our gas scintillation tests are described elsewhere.[39] A description of the layout of the target is given in references 6, 7, and 39, and is not repeated here.

B. Muon Beam

Mesons were produced by inserting a 2-in.-thick beryllium target into the 720-MeV internal proton beam of the Lawrence Radiation

Laboratory's 184-inch synchrocyclotron. The particles were deflected out of the cyclotron by its magnetic field into a quadrupole magnet. This quadrupole brought the beam to a focus where the beam's energy was degraded by 10.6 in. of polyethylene. A bending magnet then selected a momentum of 109 MeV/c so that the muons would have the correct range to traverse the material in front of the helium gas.[40] Finally a second quadrupole brought the beam to a second focus at a collimator with a 2.5-in. aperture placed just before the helium target.

Two time-of-flight counters (B1 and B2) with their associated electronics analyzed the beam into pions, muons, and electrons. The fast coincidence circuit[41] Bμ produces an output pulse whenever a particle has the correct time-of-flight between B1 and B2. The input signals to Bμ are monitered independently of whether or not a coincidence is made. These monitor signals are used to start and stop a fast transistorized time-to-pulse-height converter[42] whose output goes to a PHA.[43] This time sorter allows us to measure accurately the number of pions, muons, and electrons in the beam.[44]

Two criteria were used in experimentally optimizing the beam: (a) muon intensity, and (b) the ratio of μ to (π+e). Under the best conditions we obtained 650 muons/sec (≈ 57% of the beam particles were muons) incident on the target. A momentum dispersion of $\Delta p/p \approx 4.4\%$ resulted in ≈ 50 muons/sec stopping in the helium gas (at 28.9 atm) and to an events rate of ≈ 10 triton recoils per minute. The beam duty factor was typically 0.55. Positive muons were obtained by the reversal of all the magnetic fields and the use of the particles emitted in the backward direction from the cyclotron target. Typical μ^+ intensities were ≈ one quarter of the negative-muon intensities.

C. Stopping-Muon Identification

Identification of muons stopping in the helium gas proceeds as follows. The pulse from the Bμ coincidence is amplified, scaled, and fed into the coincidence circuit Sμ.[45] The dynode pulse from the He counter (4) is split, amplified, delayed, and fed from a discriminator into Sμ. Thus a He-Bμ coincidence ensures that a muon reached the helium gas. To ensure that the muon did not go beyond the helium gas, the cup counter's anode signal (5) is used as a veto in Sμ. Another anticoincidence turns the circuit Sμ off for 22 μsec after every beam muon enters the system. This inhibit keeps the rest of the electronics from being "confused" when there is a pileup of muons and vetoes about 2.5% of all the Sμ.

To prevent the possibility that a good event might not be analyzed because the analyzer is already busy, the PHA also inhibits Sμ during the time it is analyzing a pulse. To first order these two inhibits do not affect the T/Sμ ratio since they inhibit equally muons that are going to be captured or those that will decay.

Some good stopped muons decay almost immediately; their decay electron then has a good chance of causing a pulse in $\bar{5}$ to veto the coincidence Sμ. This would tend to increase the T/Sμ ratio since this effect preferentially vetoes those muons that decay into electrons. From a measurement of the overlap of the anticoincidence $\bar{5}$ pulse with the coincidence HeBμ, we calculate that 0.55 ± 0.11% of all stopped muons are vetoed by their own decay electrons.

The output of the circuit Sμ is scaled twice, once directly out of Sμ and once after a discriminator set to fire on all Sμ pulses. Another output of Sμ starts a time-to-pulse-height converter that is stopped either by a μ-e event or by a TR event. In addition, the circuit Sμ generates a 6.2-μsec pulse used to gate the coincidence circuit TR.

D. Distribution of Stopping Muons

Knowledge of the spatial distribution of muons stopping in the target is needed for one to properly calculate the following quantities:

a. The fraction of the muon beam stopped in the target,

b. The fraction of the muon beam stopped in the dead layer of the cup counter (see Sec. IV. A),

c. The fraction of muons stopping in the gas but close enought to the wall so that the triton recoil collides with the wall (see Sec. IV. I),

d. The fraction of muon-decay electrons that escapes counters 3 and 5 (see Sec. III. E),

e. The energy distribution of the charged particle in the breakup reactions, Eqs. (4) and (5) (see Sec. IV. F).

The stopping-muon distribution is mainly determined by the size of the collimator just before the target and by the occurrence of multiple scattering as the muon slows down in the material before the gas. The distribution was both calculated and experimentally measured. In calculating the multiple scattering we followed the method given by Sternheimer,[46] and obtained the density distributions shown by the dashed lines in Fig. 4. Because of the spreading of the beam, about 50% more muons stop in the front of the gas than in the back. In order to verify the multiple-scattering calculation, three Ilford K-5 nuclear emulsions (600 μ thick) were exposed inside the target. Within the limited scanning statistics it appeared that the beam was cylindrically symmetric and that the stopping distribution checked well with the multiple-scattering calculation (see Fig. 4).

E. Decay-Electron Detection

Most of the stopping muons decay into electrons. Some of these electrons are detected by the μ-e coincidence circuit as follows. A pulse from Sμ, signifying a stopped muon, fires a discriminator that generates a 10.6-μsec pulse. This pulse makes a coincidence in the μ-e circuit[45] with a signal coming from either counter 3 or counter 5. Since all beam particles trigger a pulse in counter 3 as the muon stops, the 10.6-μsec pulse from Sμ is delayed 35 nsec from a coincidence with such prompt pulses. Thus μ-e is sensitive from 35 ± 7 nsec to 10.6 μsec after a muon stops, and will detect only 97.6 ± 0.4% of the electrons because of this time gate. The geometric efficiency for detecting a decay electron in counter 5 (computed by the Monte Carlo program) is 85.6 ± 0.5% of the Sμ counts. Taking into account the finite-time gate and the small fraction of captured muons, one expects to observe 82.8 ± 0.6% decay electrons in counter 5. Experimentally 82.5 ± 0.3% decay electrons were observed if 2.1% random events are subtracted from the μ-e coincidences. The two numbers compare well and give a useful check of the Monte Carlo program and $\bar{5}$ efficiency.

Because of its small solid angle and because many of the decay electrons stop in the front Lucite window, the copper elbow, or the pressure-vessel flange, counter 3 detects only 1.9 ± 0.5% of the decay electrons. Considering that counter 3 has a rate of randoms as high as 3.1% of Sμ, it does not appear that counter 3 is very useful as an electron detector, which was its original purpose. As it turned out, the main reason for using counter 3 was as a veto in the circuit TR. Here it vetoed about 2% of the beam particles that otherwise would appear as random background on the TR pulse-height spectrum.

The μ-e circuit has three outputs. The first goes to a scaler, which counts μ-e events; the second goes to the μ-e logic system; and the third stops a time sorter started by an Sμ coincidence. From the time analysis we obtained a muon mean life of 2.19 ± 0.03 μsec, which agrees well with the expected 2.189-μsec characteristic of negative-muon decay in He^3.

The rationale of the μ-e logic system follows. A given muon can "die" only once. Therefore, if a muon decays into an electron there can be no capture event and one should not look for such events on the pulse-height analyzer. Ideally one could not get a TR event and a μ-e event for the same Sμ. However, random events not connected with an Sμ do occur in both TR and μ-e. The μ-e logic system is designed to eliminate ≈ 84% of the randoms occurring in the pulse-height spectrum by requiring that no TR event can register on the PHA if a μ-e event occurs in the first 10.6 μsec after a stopped muon.

This logic system was used only on one short trial run for two reasons: (a) randoms in the pulse-height spectrum were smaller than expected and could be measured in any event (see Sec. IV. D) and (b) random events in μ-e itself led to the cancellation of good triton-recoil events. From the measured random events in μ-e, analysis showed that we must correct the observed number of TR events by the factor 1.04 ± 0.01, if the μ-e logic system were used.

F. Triton-Recoil Detection

Muon-capture events are detected in the triton-recoil circuit as follows. The 6.2-μsec pulse from Sμ forms a delayed coincidence in the circuit[45] TR with pulses coming from the dynode of the He counter.

(The He anode signal is analyzed according to pulse height if there is a TR coincidence output.) The 6.2-μsec pulse is delayed from a prompt coincidence to prevent the stopped-muon pulse in the helium counter from registering in TR. Any $\bar{3}$ or $\bar{5}$ pulse occurring within ≈ 20 nsec of a He pulse vetoes the TR event. This anticoincidence prevents many of the decay electrons and all second beam particles from registering on the PHA; some capture events in which the charged particle has enough energy to leave the gas are also vetoed. Triton recoils have a small range and are not vetoed. Random $\bar{3}$ or $\bar{5}$ pulses veto ≈ 0.025% of the true TR events.

There are three outputs of the circuit TR. The first goes to a scaler. The second output is a 160-nsec pulse that gates the He anode pulse going to the PHA. The third output stops a time sorter started by Sμ; thus we can measure the characteristic time distribution of TR events. Of the normal TR events, almost 80% were actually low-energy pulses due to decay electrons that missed being vetoed. Usually we measured the time distribution of all TR events simultaneously with the pulse-height analysis; however, in one run in order to measure the time distribution of nuclear-capture events only, we set the TR discriminator to bias out events with energy below 1.2 MeV. In this run we obtained a muon mean life of 2.23 ± 0.08 μsec, thus verifying that the effect we measure is related to a muon stopping in helium.

It is important to know between what time, t_1 to t_2, after a stopped muon that a He pulse will register in TR. Since triton recoils follow an exponential law with mean life τ = 2.189 μsec (the inverse of the muon-disappearance rate in He^3), one must correct the observed events for those that come before t_1 or after t_2. We measured the time t_1 by "doing" a delay curve between the prompt stopping muon He pulse

and the Sμ coincidence pulse. An additional delay length of 202 ± 3 nsec was then added to delay the Sμ pulse from the point where TR counts at half efficiency. The time $t_2 - t_1$ equals the Sμ pulse length and was measured on a calibrated oscilloscope to be 6.2 ± 0.1 μsec. The fraction of muons disappearing between t_1 and t_2 is

$$F_t = \exp(-t_1/\tau) - \exp(-t_2/\tau) = 0.858 \pm 0.003, \qquad (28)$$

and the total number of events occurring over all times is the observed events divided by this fraction.

G. Pulse-Height Analysis

Delayed pulses from the He counter's anode are sorted according to energy (pulse height) in order to pick out pulses arising from the 1.9-MeV triton recoil. To prevent saturation of the pulses in the last stages of the photomultiplier tube, the voltage of the He counter was kept relatively low. An amplifier compensated for this low voltage in order to make the pulse through the gating circuit an optimum volt or so. The He anode signal was delayed so that it fell within the gating pulse provided by the TR circuit, which in turn was generated by He's dynode signal. The integrating amplifier[47] that followed the gating circuit integrated the area of the pulses, and produced an output-pulse height proportional to the total amount of light generated in the helium gas. Finally the pulses were analyzed according to pulse height in the PHA.[43] The resulting pulse-height spectra, along with the Sμ scaler counts, are the basic data of the experiment.

Frequent energy calibrations of the PHA were made with an Am^{241} α source. The pulse-height-analysis system was linear up to PHA channel 110, where the integrating amplifier saturates (see Fig. 5 of

reference 39). Because of the electronic saturation, large pulses, which normally would be off-scale on the PHA were instead stored in the PHA between channels 120 and 134. Thus no matter how large the He pulse, it still registered on the PHA. These saturated pulses were used in obtaining the capture rates for the breakup reactions.

Figure 5 (a) through (h) shows the raw pulse-height spectra for each set of data. Pulse-height spectra with He^3 in the target were taken in five main runs, during which the experimental conditions were varied to check for systematic errors.[48] Run A was made at the beginning of data gathering and Run B about 2 weeks later; otherwise these two runs were made under identical conditions at 28.9 atm of He^3. The only change made during the LP (low-pressure) run was the lower gas pressure at 15.4 atm. During the logic run the μ-e logic system (see Sec. III. E) was used. In addition, run B3 was made without $\bar{5}$ in the TR coincidence and with a 2:1 attenuator before the linear amplifier. This made it possible to see more of the breakup reactions [Eqs. (4) and (5)] since the breakup proton and deuteron have relatively high energies and many normally veto themselves in counter 5.

Two main runs were made with He^4 in the target. The first, B4, was identical to B3 except for the gas used, and was an effort to observe capture events in He^4 [Eq. (8)]. Since the objective of the second He^4 run (C) was to study the electron and breakup backgrounds, it was made under conditions similar to Runs A and B. In addition, a run with positive muons was made in order to check the shape of the electron background.

The energy spectra of Fig. 5 (a) through (e) all show the 1.9-MeV triton-recoil peak. We want to know the number of counts in this peak in order to calculate the $He^3 \rightarrow H^3$ capture rate. Three major backgrounds

complicate the computation of the capture rate. The sharply rising background at low energies is from μ to e decays in which the electrons miss the veto counters (see Sec. IV.E). Random background (the dots in Fig. 5) was measured to an accuracy of $\approx$ 15% and is discussed in Sec. IV.D. The remaining background is due mainly to muon capture resulting in many-body final states [Eqs. (4) and (5)]. This breakup background contributes the largest uncertainty in the determination of the number of triton-recoil counts; however, a measure of it determines the total capture rate in He^3. The runs with μ^- stopping in He^4 [Fig. 5 (f) and (g)] of course do not show any recoil peak but have a spectrum similar to the He^3 case in other respects. The run with μ^+ on He^3 has only the decay-electron background as it should since positive muons are not captured.

Initially an attempt was made to separate the triton peak from the background by fitting the spectra to a shape consisting of two Gaussians plus a linear background. The low-pressure data form the only spectrum that fitted well. The logic data were on the border line; but the χ^2 for runs A and B represent especially bad fits. A close inspection of the spectra in Fig. 5 (a) and (b) reveals that the triton peak in asymmetrical for A and B, and thus could not be expected to fit a Gaussian shape. A Poisson shape fits the triton peak even less well. Consequently, except for the LP data and possibly the logic data, shape fitting does not lead to trustworthy results and was not used in the final data analysis. It is comforting to note, however, that the results of the LP and logic-curve fitting agree exceedingly well with the final triton-count determination (see line 2 of Table IV).

IV. DATA ANALYSIS

In this section we describe how the data were analyzed and calculate the capture rates in He^3 and He^4. We first describe the xenon analysis and then compute the number of muons stopping in the helium gas for each run. Next we discuss the backgrounds of the pulse-height spectra, and give a short description of the Monte Carlo program used in analyzing the breakup events. Then we calculate the capture rate in He^4 and the breakup-capture rate in He^3. Consideration of events arising from muon capture in the walls shows these to be a factor in the breakup capture rates. After making a correction for triton recoils that hit the wall of the gas container, we finally arrive at the $He^3 \rightarrow H^3$ capture rate.

A. Xenon Analysis and the Dead-Layer Correction to Sμ

Not all of the muons that register in the coincidence circuit Sμ actually stop in the helium gas. Some muons stop in the "dead layer" that surrounds the gas, that is, in the cup-coating materials or in the cup counter itself. Most muons that stop in the cup counter veto themselves in Sμ; however some do not penetrate deeply enough into the cup counter to give sufficient light to be vetoed. These muons must be subtracted from the Sμ counts in order to get the true number of muons stopping in the helium. This correction was determined experimentally by replacing the helium with xenon gas and performing a time analysis of $\mu \rightarrow e$ decays (see Sec. III. E). Figure 6 shows a typical time distribution of μ-e events with xenon in the target. Muons stopping in xenon have a very short mean life (90 nsec),[49] whereas muons stopping in the low-Z materials of the dead layer have mean lives of about 1 μsec. Using this spectrum to determine the number of muons stopping in the dead layer is rather involved, but the following outlines how it was done.

The "dead layer" consists principally of four elements: magnesium, oxygen, aluminum, and carbon. The MgO powder was "smoked" onto the cup-counter walls over an opaque coat of Al. The MgO had an average thickness of 0.93 ± 0.04 mg/cm^2; the Al, 0.09 ± 0.03 mg/cm^2. From the time distribution (Fig. 6) one can see that it would be very difficult to extract the number of muon stops in all four elements. Since we measured the amount of MgO and Al present, we first determined how many counts corresponding to stops in MgO and in Al one would expect to see in the time distribution. This MgO and Al contribution was subtracted and a least-squares fit made with the remaining spectrum assumed to consist of a constant random background and two exponentials, one with the xenon and the other with the carbon lifetime. In this calculation it was assumed that muons captured in the dead layer do not cause a signal in counter 5. The electron-detection efficiency, the muon mean life in each element,[50] and the stopping-muon distribution were taken into account.

The number of muons stopping in the dead layer should be independent of the gas pressure and directly proportional to the number of incident-beam muons (Bμ). In order to help detect systematic errors, runs were made at various xenon pressures. Averaging these runs, we obtained $(2.3 \pm 0.3) \times 10^{-3}$ dead-layer stops per Bμ. This is the number used in correcting the scaler Sμ counts and corresponds to a dead-layer thickness of about 2.2 mg/cm^2 (equivalent of C) or about 1.1 mm of He^3 gas at 28.9 atm. Checks showed that the dead-layer correction is relatively insensitive to the MgO and Al subtraction, and that the dead layer is insensitive to small changes in the high voltage or amplifier gain of counter 5.

B. Number of Stopping Muons

Table II lists the pertinent numbers used in calculating the number of muons stopping in the helium gas for each of the runs. The discussion in Sec. IV. A demonstrated that $[(2.3 \pm 0.3) \times 10^{-3} \times (B\mu \text{ scalar counts})]$ muons are expected to stop in the dead layer surrounding the gas; these are subtracted from the $S\mu$ scaler counts. To this we add that fraction of the muons that are vetoed by their own decay electrons (see Sec. III. C) to obtain the final corrected number of stopping muons. Note that the errors are $\approx 0.5\%$ at the high gas pressure and $\approx 1\%$ at the low gas pressure. The "dead-layer" correction contributes the largest part of this error. Other possible corrections to $S\mu$ were investigated and rejected as negligible. Besides the time-of-flight requirement, pions and electrons in the beam should not stop in the helium because of range considerations.

C. Muon-Capture Events in the Wall

We now estimate the number of muons stopping in the dead layer that give a good TR event. Because muon-capture rates are higher in heavier elements, these wall events could contaminate the desired energy spectrum of muons stopping in helium. Knowing the number of muons stopping in the dead layer per $B\mu$ (Sec. IV. A) and the capture rate in each element,[50] we calculate that $4.3 \pm 1.3 \times 10^{-4}$ wall captures occur per $B\mu$ within the TR time gate. The capture products consist mainly of neutrons and gamma rays. Charged capture products are neglected here and discussed further in Sec. IV. H. The gamma rays will not be detected, as their secondary electrons leave little energy in the helium. The major portion of false TR events are expected to come from neutrons that collide elastically in the gas. Note that wall events are inversely proportional to the pressure for charged products but independent

of the pressure for neutral products. A Monte Carlo program used a typical theoretical neutron spectrum[23] and a neutron multiplicity per capture of 1.0 ± 0.3,[51] folded in the geometry (solid angle) of the helium scintillator, and used total[52] and differential[53] n-He cross sections to provide the energy spectrum of recoil helium nuclei (Fig. 7). About 1.3% of the capture products interacted in the helium at high pressure and $\approx 0.7\%$ at low pressure, but only about a fifth of these had energies above the electron background. These gave the number of wall events listed on line 3 of Table III. These numbers are small compared to the observed events, but they are not quite negligible, especially in the He^4 case in which they amount to about 5% of total events.

D. Random Background

The random background of the pulse-height spectra of TR events was measured by allowing the TR coincidence to fire on every He pulse. Thus, we obtained the pulse-height spectrum of singles in the He counter and were able to compute the random spectrum to be subtracted from the raw data (see Fig. 5). These singles runs were made every few hours after $\approx 10^6$ Sμ. We estimate the uncertainty in the beam duty factor to be $\approx 15\%$ and, since other quantities have smaller errors, this is also the error in the randoms calculation (see line 3b, Table IV).

Most of the random events arise from thermal neutron reactions in He^3 according to

$$n + He^3 \rightarrow H^3 + p \,. \tag{29}$$

This reaction releases 0.77 ± 0.02 MeV and accounts for the peak in the random spectrum with He^3 gas in the target. The runs with He^4 in the target show that the remaining random background is rather flat, except

for a low-energy tail that may be associated with tritium decays but more likely is due to other neutron reactions. Note that random charged particles should not constitute a background since in general they are vetoed in counters 3 or 5.

E. Decay-Electron Background

Considerable uncertainty in determining counts on the low-energy edge of the triton peak is introduced by the decay-electron background, which rises sharply until it is artificially cut off at ≈ 0.4 MeV by a discriminator. This background is due to electrons (from muon decay) that miss being vetoed in counters 3 or 5 and thus arises mostly from the 15% of the electrons that pass through the front hole in the cup counter.

The shape of the electron background that is to be subtracted from the pulse-height spectra was established from the runs μ^+He^3 and μ^-He^4. The procedure followed was to subtract the capture events from the μ^-He^4 data (run C) and normalize the resulting "electron tail" to the same number of $S\mu$ as each of the other appropriate runs. The resulting spectrum agrees reasonably well with the μ^+He^3 data and with the gross shape of the electron background in runs A and B, and thus it was subtracted from runs A and B; this left only the triton peak and the breakup background. Similarly, run B4 was subtracted from run B3. In the case of the low-pressure and logic runs there were no accompanying μ^-He^4 or μ^+He^3 data and the electron background was obtained by curve-fitting a Gaussian tail. Because the electrons lose less energy in the gas at low pressure, there was good separation between the TR peak and the electrons in the LP run, and the error associated with uncertainties in the electron background in the LP run is small. Estimates of the error introduced in the triton counts are tabulated

on line 3c of Table IV. Because the electron background is so large, any determination of the number of breakup events below ≈ 1.5 MeV is impossible.

F. Monte Carlo Program

In order to properly calculate the breakup background and to find the shape of the breakup-energy spectrum, it is necessary to account for a number of factors. Among these are the distribution of stopping muons, the energy resolution of the He counter, energy lost by the charged particle in the helium gas, the energy distribution of breakup events, and the probability that the charged breakup particle vetoed itself in counter 5. The most practical method of combining these factors to give a breakup shape is through a Monte Carlo program that simulates events. The program takes a theoretical breakup energy distribution and folds in the above factors. Figure 8 shows the effect of these factors on a phase-space-energy distribution[54] of the deuteron in the reaction $\mu^- + He^3 \rightarrow d + n + \nu$. One can see the effect of the finite size of the gas scintillator, since in the output spectra there are no particles with range greater than 5 inches. The higher energy particles leave only a part of their energy in the gas and then most pass into counter 5 with enough energy to veto themselves. During the runs (B3 and B4) where counter 5 was not used as a veto in TR, these higher energy particles would still show up on the spectrum but shifted to a lower energy. With counter 5 veto on, none of these particles would show up on the observed energy spectrum. Similarly at the lower gas pressure, the particles leave even less energy in the gas and more veto themselves.

G. Calculation of the Muon-Capture Rate in He^4

Figure 9 shows the data with randoms subtracted for run B4 with He^4 in the target; run C is similar. Only the spectra between 1.5 MeV, where the decay-electron background becomes large, and channel 115, where the pulse-height-analysis system begins to saturate, was observed directly, and these points are shown on the graph. In addition to these points, however, the total number of events above channel 115 was measured (see Sec. III. G). The number of events observed in each energy region is tabulated in the box on the graph, and the total observed events are listed on line 2 of Table III. The wall events (Sec. IV. C) are subtracted from line 2 to give the number of observed events in the helium. The remaining question is how many events lie in the region below ≈ 1.5 MeV masked by the electron background.

To determine these unobserved events, a theoretical energy spectrum for the triton of Eq. (8)[23] (called Bietti's spectrum for convenience) was modified by the Monte Carlo program (Sec. IV. F) and normalized to the observed number of capture events. The resulting shape (the solid curve of Fig. 9) agrees well with the data and gives the number of unobserved events under the electron background (line 4 of Table III). Other shapes would also fit the limited data but grossly different shapes, e.g., a phase-space distribution (the dashed line in Fig. 9), do not. It is difficult to assign an error to the unobserved events; however, a ±25% variation would be reasonable if one considers the relatively good fit of the theoretical shape to the data. It must be emphasized, however, that we have no experimental information in the low-energy region of the spectrum.

Two additional factors complicate a determination of the capture rate in He^4. Besides reaction (8), possible reactions include:

$$\begin{aligned} \mu^- + He^4 &\rightarrow H^3 + n + \nu + \gamma \\ &\rightarrow H^2 + 2n + \nu \\ &\rightarrow H^1 + 3n + \nu . \end{aligned} \tag{30}$$

In this experiment, we can not distinguish tritons, deuterons, or protons, but can detect only the energy of charged particles irrespective of their mass. We neglect the effect of these other reactions (30) in determining the unobserved events because reaction (8) is expected to occur 90% of the time.[21] The second factor that changes any straightforward calculation of Λ is the presence of events in the pulse-height spectrum that are derived from charged wall events. These are not accounted for here but are discussed in Sec. IV.H.

With the above reservations, the muon-capture rate in He^4 can now be calculated. In run C the total number of events must be corrected for the 5% that veto themselves in counter 5. This fraction is determined by the Monte Carlo program and depends on the assumed theoretical-energy distribution. In addition to this factor, the total number of events is multiplied by 1.1655 ± 0.004 to correct for the finite TR time gate (see Sec. III.F). The corrected total number of events is listed on line 6 of Table III. Dividing by the number of stopped muons and multiplying by the free muon-decay rate then gives the muon-capture rate in He^4 [see Eq. (7)]. The two runs are in excellent agreement and average to give a capture rate of

$$\Lambda\,(He^4) = 375 \pm 30\ \text{sec}^{-1}. \tag{31}$$

It must be stressed that the error is almost entirely due to the uncertainties in the "unobserved" events and thus is only an estimate.

H. Calculation of the Breakup Capture Rate in He^3

The calculation of the capture rates for the breakup reactions [Eqs. (4) and (5)] proceeds similarly to the He^4 calculation. However, there are two additional complications with the He^3 calculation: (a) an even greater portion of the low-energy spectrum is masked since the triton peak covers the spectrum from ≈ 1 to 3 MeV, and (b) the branching ratio between the proton and deuteron reactions above is unknown experimentally. Yano obtained a theoretical branching ratio of ≈ 3 deuterons to 1 proton,[4] and Messiah[55] calculated rates for similar pion-capture reactions

$$\begin{aligned} \pi^- + He^3 &\rightarrow d + n + \gamma \\ &\rightarrow p + 2n + \gamma \end{aligned} \tag{32}$$

and obtained a branching ratio of ≈ 4 to 1. For the purpose of analysis of the unobserved events, we used a branching ratio of 3.5 to 1. There are no theoretical calculations of the proton spectrum in reaction (5), but it is expected to be similar to the deuteron spectrum after the differing masses are taken into account.

Yano has also computed the energy distribution of the deuteron in reaction (4) in the c.m. system of the three nucleons.[56] Transforming to the laboratory system, we obtain the spectrum shown in Fig. 10 (called the Yano spectrum for convenience). If allowance is made for the deuteron-triton mass difference, Bietti's spectrum[23] can also be applied to reaction (4). This shape is also shown in Fig. 10. Note that the shapes differ considerably below ≈ 1 MeV, but are similar in the observable region above

the triton peak. As far as the experimental data are concerned, one shape is as good as the other and a normalized average of the two shapes (solid line in Fig. 11) was used to compute the "unobserved" events below ≈ 3 MeV (line 4, Table III). A 50% error was assigned to these unobserved events since it did not appear that the events below 3 MeV could vary by more than this.

By adding the observed and unobserved events for each run in Table III, correcting for the number of breakup events that veto themselves, correcting for the finite TR time gate, and dividing by the number of stopped muons, one obtains the total number of events per Sμ. From Eq. (7) and $\Lambda_C \approx 1500\ \mathrm{sec}^{-1}$, one obtains $\Lambda_B = 4.56 \times 10^5$ (events/Sμ events). The breakup capture rates for each run are shown on line 9 of Table III. The weighted average of the four runs is

$$\Lambda_B = 700 \pm 180\ \mathrm{sec}^{-1}, \tag{33}$$

where again the error is mostly from the uncertainty in the "unobserved" events. Note, however, that the low-pressure run gives a high Λ_B well outside the statistical errors (but not outside the error quoted, which is due to the systematic uncertainty of the unobserved events). This discrepancy is disturbing, for it would indicate a systematic error in all the breakup results.

It can be argued that the serious discrepancy of the LP-breakup-capture rate arises from wrong assumptions concerning the "unobserved" events; however, the observed events by themselves also show this discrepancy. We have three possible explanations for the discrepancy: (a) if by some blunder the $\bar{5}$ veto to TR was off during the LP run there would be no correction for vetoed events and $\Lambda_B(\mathrm{LP}) = 660\ \mathrm{sec}^{-1}$ is in excellent agreement with the HP runs; (b) if the assumed theoretical

shape (Fig. 10) were skewed very much toward low energies, the calculated fraction of vetoed events would become closer to unity and the discrepancy would decrease; and (c) if ≈ 19% of wall capture events give charged particles--protons and alphas--as reaction products (neutral particles were discussed in Sec. IV. C), the HP and LP breakup rates are both equal to 400 sec^{-1}, that is 40% of Λ_B (HP) must result from muon-capture events in the walls to account for the discrepancy. To our knowledge the fraction of charged particles coming from muon capture in Mg, O, C and Al has not been measured, but it is not inconceivable that ≈ 19% of the products are charged. However, in an emulsion study only 2.5% of the products were charged;[57] thus offhand one would tend to disbelieve such a large fraction. Neglecting blunders, one must conclude that the breakup capture rates have not been measured with as great an accuracy as given in Eqs. (31) and (33) and the values given there are upper limits only. The LP discrepancy is probably due to a combination of (b) and (c) but with the present information it is not possible to calculate either of these factors. If we assign lower limits to the breakup rates in He^3 and He^4 by assuming that 19% of charged wall capture events could be present, and if the LP data is not averaged in, we obtain

$$\Lambda_B = 665^{+170}_{-430}\ sec^{-1}, \tag{34}$$

$$\Lambda\ (He^4) = 375^{+30}_{-300}\ sec^{-1}. \tag{35}$$

I. Triton-Recoil Edge Correction

Luckily the LP discrepancy does not appreciably affect the $He^3 \rightarrow H^3$ capture rate. However, one other correction--the triton recoil-edge correction--must be discussed before the $He^3 \rightarrow H^3$ capture rate can be calculated.

Some muons will stop near the edge of the helium gas near the cup counter; if they are captured, their triton recoil could lose most of its energy in the wall materials and not give enough light in the helium to be detected by pulse-height analysis. Table V lists the energies at which one would expect the triton to have a 10%, 50%, and a 90% chance of being observed in the pulse-height spectra. For each energy, the distance the triton must travel in the helium to deposit that energy is also given. Assuming an isotropic angular distribution, and taking the distribution of stopping muons into account, the Monte Carlo program then calculated how many tritons would be lost in the wall for both pressures at which data were taken (line 4, Table V). Taking the central values as the correction with errors given by the 10/90% limit, we must then correct the observed triton recoils by $0.9 \pm 0.3\%$ at 28.9 atm and by $1.7 \pm 0.5\%$ at 15.4 atm. The correction at the lower pressure is larger since the tritons travel further at the lower pressure and more have a chance of hitting the wall.

J. Calculation of the $He^3 \rightarrow H^3$ Capture Rate

The major goal of this experiment was the measurement of the muon-capture rate, Λ_C, in reaction (3). Its calculation is now discussed. First, the random and electron backgrounds were subtracted from the basic pulse-height spectra of Fig. 5 (a) through (e). The breakup background was subtracted by use of the solid curve in Fig. 11 with errors shown by the dotted lines (Sec. IV.H). Finally the remaining counts were added to give the observed triton-recoil events shown on line 2 of Table IV. The errors contributed by each source are listed on line 3 of Table IV.

These observed triton-recoil events must then be corrected for the number lost in the walls (Sec. IV.I) and for the finite TR time gate (Sec. III.F). In addition, the logic data must be corrected for good TR events that are vetoed by the μ-e logic system (Sec. III.E). The total correction factor applied in each case is listed on line 4 of Table IV, the corrected number of triton recoil counts is shown in line 5. The capture rates are computed from Eq. (6) and are listed on line 8 of Table IV. Errors from each source are treated independently for each run. Weighting each result by the inverse square of its errors gives an average capture rate for the five runs of

$$\Lambda_C = 1505 \pm 46 \text{ sec}^{-1}. \tag{36}$$

The error in this averaged result arises mostly from the uncertainty in the breakup backgrounds and is obtained by dividing the error for each run into a systematic and a random part. The random part, consisting of lines 3a, b, and c in Table IV, is then treated independently for each run. There is excellent statistical agreement among the five runs, because the χ^2 (with only the random part of the error used) is 3.33 (50% chance of occurrence).

V. RESULTS AND CONCLUSIONS

This muon-capture experiment yields the capture rates in He^3 and He^4. The final results are listed in Table I. The breakup capture rate in He^3

$$\Lambda_B(He^3) = 665^{+170}_{-430} \text{ sec}^{-1} \tag{34}$$

is combined with the $He^3 \rightarrow H^3$ partial rate

$$\Lambda_C(He^3 \rightarrow H^3) = 1505 \pm 46 \text{ sec}^{-1} \tag{36}$$

to give a total muon-capture rate in He^3 of

$$\Lambda(He^3, \text{total}) = 2170^{+170}_{-430}\ \text{sec}^{-1}. \tag{37}$$

The total capture rate in He^4 is measured to be

$$\Lambda(He^4) = 375^{+30}_{-300}\ \text{sec}^{-1}. \tag{35}$$

Note the large isotope effect. The large lower limits for the He^3 breakup rate and the He^4 total rate signify the possibility that some of the events may have been from muon captures in the wall surrounding the gas. The error in the $He^3 \rightarrow H^3$ rate is almost entirely due to the uncertainties in the breakup capture events. All of the errors could be reduced in a rerun of this experiment, for the methods used are capable of giving very accurate results.

If the wall events are small, the He^4 capture rate agrees with the previous measurements and the theoretical predictions (see Table I). Similarly the total He^3 capture rate is in excellent agreement with a previous measurement by Falomkin et al.,[8] who used a helium-diffusion chamber. The old theoretical prediction by Primakoff[13] agrees reasonably well with the measured total capture rate; Yano's recent and more detailed calculation of the breakup capture rates[4] is in excellent agreement with the observed value.

Although our measurement of the $He^3 \rightarrow H^3$ capture rate is the highest obtained in the three experiments performed so far, it does not disagree with the other results. Except for the calculations of Duck[20] and Fujii,[19] the theoretical predictions are in agreement with our result. The theoretical prediction of the $He^3 \rightarrow H^3$ capture rate is uncertain to 10% because of ambiguities in both the He^3 rms radius and g_p (the induced pseudoscalar coupling constant).

If the experimental value of the $He^3 \rightarrow H^3$ capture rate is substituted into $\Lambda_C = 1/4\ \Lambda_s + 3/4\ \Lambda_t$ (Λ_s and Λ_t are given by a modification of Adam's formula[37] with S = T = 0), one obtains a relation between the two most uncertain parameters in muon capture--P and A. Figure 12 is a plot showing this relation. The intersection of $g_P = 6.6A_\beta$ with band I is in good agreement with the experimental capture rate. However, Λ_t is quadratic in P and has a minimum in the region of interest. Thus, with the inclusion of the uncertainties in $A(q^2)$ any value of g_P between 0 and +25 A_β is allowed. Several recent experiments have indicated a value of g_P closer to 15 A_β,[35,36] indicating that band I is correct. A graph similar to Fig. 12 is given by Rothberg et al. for muon capture in hydrogen.[2,58]

This experiment does not rule out the possibility of a (V + A) interaction in muon capture. For a V + A interaction and for a capture rate of 1505 sec^{-1}, one obtains the dashed curve in Fig. 12. Note that it too is consistent with $g_P = +6.6\ A_\beta$.

The present uncertainties in A and P, not to mention S and T, make an accurate verification of the universal Fermi interaction hypothesis difficult. These difficulties arise because of the presence of strongly interacting nucleons and because of the large momentum transfer involved in muon capture. There are so many parameters that practically any capture rate near 1500 sec^{-1} can be calculated with an appropriate choice of the coupling coefficients. Only if both S and T are zero is there hope verifying UFI to any accuracy less than 10%. Nonetheless the excellent agreement between the theoretical and experimental values of the capture rates in helium lends considerable support to the hypotheses of a universal Fermi interaction and a conserved vector current.

ACKNOWLEDGMENTS

We are pleased to acknowledge the support and interest of Prof. Emilio Segrè, the advice of Prof. Norman E. Booth, and the sustained effort of the target group--in particular William L. Pope, Richard V. Schafer, and Raymond Z. Fuzesy--who engineered and tested the high-pressure gas target. The crew of the 184-inch cyclotron maintained a steady and reliable beam throughout the experiment. We also wish to thank the many other staff members of the Lawrence Radiation Laboratory whose generous support made this experiment possible.

APPENDIX

Advantages and Disadvantages of Muon Capture in Hydrogen

Much data are available on muon-capture rates in complex nuclei,[49,50] but the data are difficult to interpret because of the many strongly interacting nucleons and many final states. Ideally, therefore, one would like to study the muon-capture rate in hydrogen[2] where there are no nuclear-structure effects. There are, however, five main reasons why an experiment in He^3, the next simplest nucleus not an isotope of hydrogen, is easier to perform and to interpret. These are:

1. The muon-capture rate in hydrogen is especially sensitive to whether the μ-p atom is in a triplet or a singlet hyperfine state.

2. The μ-p atom is neutral and rapidly diffuses through the hydrogen undergoing collisions with other protons. In these collisions the muon is often exchanged from proton to proton. These exchange collisions rapidly change the original statistical population of 1/4 singlet and 3/4 triplet atoms of 100% singlet μ-p atoms (the ground state of the μ-p system). Furthermore, in liquid hydrogen in about 0.5 μsec the singlet μ-p atom becomes part of a $(p\text{-}\mu\text{-}p)^+$ molecular ion, if the muon has not decayed first. In such an ion the muon can be captured by either proton, and the fraction of muons captured, with spin aligned with or opposite to the capturing proton, varies depending upon whether the $p\text{-}\mu\text{-}p^+$ ion is in a para or an ortho state. All such variations in the relative-spin states affect the capture rate. In addition, the uncertainty of the molecular wave function in the $p\text{-}\mu\text{-}p$ system causes additional theoretical difficulties in hydrogen. In helium there are no exchange collisions and the hyperfine states at capture have just their original statistical population.

3. The muon is more tightly bound to all other nuclei (including the deuteron) than it is to hydrogen. Thus any collision with an impurity nucleus has a high probability of transferring the muon from the proton to the impurity nucleus. This exchange is irreversible and, since muon-capture rates are much larger in impurities than in hydrogen, ultrapure hydrogen is required. Again this problem is not present in helium because electrical repulsion keeps the μ-He atom away from other nuclei.

4. To detect muon capture in the lighter elements one must detect the reaction product, which is a neutron in the case of hydrogen and a charged triton in the case of helium. The charged particle can be detected with virtually 100% efficiency whereas it is difficult to determine the neutron-detection efficiency.

5. Finally, the rate for observing the μ-He^3 reaction is more than 100 times that of the μ-p reaction if one includes neutron-detection efficiencies.

We conclude that the muon-capture rate in helium can be measured more accurately than the rate in hydrogen. On the other hand, for hydrogen there is no uncertainty in the nuclear structure. This one big disadvantage with capture in helium almost outweighs its favorable features. Nevertheless the hope is that the He^3 nucleus is sufficiently simple to permit an unambiguous theoretical prediction of a capture rate on the basis of a UFI.

FOOTNOTES AND REFERENCES

†Work performed under the auspices of the U. S. Atomic Energy Commission.

*Present addresses: LBA, Department of Physics, University of Pennsylvania, Philadelphia; RJE and REH, Enrico Fermi Institute for Nuclear Studies, University of Chicago, Chicago, Illinois; JTL, Physics Department, Yale University, New Haven, Connecticut; NHL, Rutherford High Energy Laboratory, Didcot, Berkshire, England.

1. E. Fermi and E. Teller, Phys. Rev. 72, 399 (1947).

2. For information on muon capture in hydrogen see J. E. Rothberg, E. W. Anderson, E. J. Bleser, L. M. Lederman, S. L. Meyer, J. L. Rosen, and I-T. Wang, Phys. Rev. 132, 2664 (1963), and references cited therein.

3. The following references summarize work done on the muon-capture interaction: R. D. Sard and M. F. Crouch, Nuclear Interactions of Stopped μ-Mesons, in Progress in Cosmic Ray Physics, edited by J. G. Wilson (North-Holland Publishing Company, Amsterdam, 1954) Vol. 2.

   L. Wolfenstein, The Muon Absorption Interaction, in Proceedings of the 1960 Annual International Conference on High-Energy Physics, Rochester, N. Y. (Interscience Publishers, Inc., New York, 1960), p. 529.

   V. L. Telegdi, Phys. Rev. Letters 8, 327 (1962).

4. A. F. Yano, Phys. Rev. Letters 12, 110 (1964).

5. G. Feinberg and L. M. Lederman, Ann. Rev. Nucl. Sci. 13, 431 (1963).

6. L. B. Auerbach, R. J. Esterling, R. E. Hill, D. A. Jenkins, J. T. Lach, and N. H. Lipman, Phys. Rev. Letters 11, 23 (1963).

7. For additional details, see R. J. Esterling, Measurements of the Muon-Capture Rate in He^3 and He^4 (Ph. D. Thesis), Lawrence Radiation Laboratory Report UCRL-11004, April 1964 (unpublished).

8. I. V. Falomkin, A. I. Filippov, M. M. Kulyukin, B. Pontecorvo, Yu. A. Scherbakov, R. M. Sulyaev, V. M. Tsupko-Sitnikov, and O. A. Zaimidoroga: Phys. Letters 1, 318 (1962); 3, 229 (1963); 6, 100 (1963).

9. R. L. Wagner, Jr., Muon Capture in Helium-3, (Ph. D. Thesis), University of Utah, 1963 (unpublished).
R. M. Edelstein, D. Clay, J. W. Keuffel, and R. L. Wagner, Jr., Measurement of the Rate for $\mu^- + He^3 \rightarrow H^3 + \nu$, in Proceedings of the Conference on Fundamental Aspects of Weak Interactions, (Brookhaven National Laboratory, Upton, N. Y.), Sept. 1963 (to be published).

10. R. Bizzarri, E. diCapua, U. Dore, G. C. Gialanella, P. Guidoni, and I. Laakso, Nuovo Cimento 33, 1497 (1964).

11. M. M. Block, T. Kikuchi, D. Joetke, M. Schneeberger, C. R. Sun, R. Walker, G. Culligan, V. L. Telegdi and R. Winston, Proc. of the Sienna Conference on Elementary Particles, Vol. 1, 26 (1963).

12. H. L. Anderson, E. P. Hincks, C. S. Johnson, C. Rey, and A. M. Segar, The Capture Rate for Muons in Helium, in International Conference on Elementary Particles, (abstract) Aix-en-Provence, 1961, Vol. 1, p. 141.

13. H. Primakoff, Rev. Mod. Phys. 31, 802 (1959). See also Ref. 22.

14. A. Fujii and Y. Yamaguchi, Progr. Theoret. Phys. 31, 107 (1964).

15. B. Goulard, G. Goulard, and H. Primakoff, Phys. Rev. 133, B186 (1964).

16. A. Fujii and H. Primakoff, Nuovo Cimento 12, 327 (1959).

17. C. Werntz, Nucl. Phys. 16, 59 (1960).

18. L. Wolfenstein, Weak Interactions: Strangeness-Conserving, in Proceedings of the International Conference on High-Energy Physics, Geneva, 1962 (CERN Scientific Information Service, Geneva, Switzerland, 1962), p. 821. The theoretical Λ_C is given here as 1400 ± 140 sec^{-1}. In a private communication to N. Lipman, Wolfenstein gives a rate of 1500 sec^{-1} based on the recently measured He^3 and H^3 form factors.[31]

19. A. Fujii, Phys. Rev. 118, 870 (1960).

20. I. Duck, Nucl. Phys. 35, 27 (1962).

21. C. A. Caine and P. S. H. Jones, Nucl. Phys. 44, 177 (1963).

22. A. Bietti, Nuovo Cimento 20, 1043 (1961).

23. A. Bietti and P. DiPorto, Nuovo Cimento 28, 270 (1963).

24. R. J. Oakes, Stanford University Report ITP-135, August 1964 (submitted to Phys. Rev).

25. For excellent reviews of the present status of weak interactions see, e.g., E. J. Konopinski, Ann. Rev. Nucl. Sci. 9, 99 (1959); W. S. C. Williams, An Introduction to Elementary Particles, (Academic Press, New York, 1961). C. S. Wu, Rev. Mod. Phys. 36, 618 (1964).

26. M. L. Goldberger and S. B. Treiman, Phys. Rev. 111, 354 (1958).

27. S. Weinberg, Phys. Rev. 112, 1375 (1958).

28. Wolfgang Drechsler and Berthold Stech, The Induced Pseudoscalar Interaction and the μ-Capture in He^3, (Institut für theoretische Physik Universität Heidelberg), preprint, September 1963.

29. R. P. Feynman and M. Gell-Mann, Phys. Rev. 109, 193 (1958). S. S. Gershtein and I. B. Zel'dovich, English trans. Soviet Phys. JETP 2, 576 (1956).

30. Y. K. Lee, L. W. Mo, and C. S. Wu, Phys. Rev. Letters 10, 253 (1963).

A. F. Dunaitsev, V. I. Petrukhin, Yu. D. Prokoshkin, and V. I. Rykalin, Phys. Letters 1, 138 (1962).

P. Depommier, J. Heintze, A. Mukhin, C. Rubbia, V. Soergel, and K. Winter, Phys. Letters 2, 23 (1962); and ibid., 5, 61 (1963).

R. Bacastow, T. Elioff, R. Larsen, C. Wiegand, and T. Ypsilantis, Phys. Rev. Letters 9, 400 (1962).

31. H. Collard, R. Hofstadter, A. Johansson, R. Parks, M. Ryneveld, A. Walker, M. R. Yearian, R. B. Day, and R. T. Wagner, Phys. Rev. Letters 11, 132 (1963).

H. Collard and R. Hofstadter, Phys. Rev. 131, 416 (1963).

32. A. Fujii, Nuovo Cimento 27, 1025 (1963).

33. For example, see reference 14.

34. Calculated by Kistner and Rustad, as reported by M. Goldhaber, Weak Interactions: Leptonic Modes, in International Conference on High Energy Physics, (CERN, CERN Scientific Information Service, Geneva, Switzerland, 1958), p. 238.

35. M. Conversi, R. Diebold, and L. di Lella, Radiative Muon Capture in Ca^{40} and the Induced Pseudoscalar Coupling Constant (paper presented at the International Conference on Weak Interactions, Brookhaven, Upton, N. Y.) Sept. 1963;

M. L. Yovnovich and V. S. Evseev, Phys. Letters 6, 333 (1963).

36. R. C. Cohen, S. Devons, and A. D. Kanaris, Phys. Rev. Letters 11, 134 (1963).

A. Astbury, L. B. Auerbach, D. Cutts, R. J. Esterling, D. A. Jenkins, N. H. Lipman, and R. E. Shafer, Nuovo Cimento 33, 1020 (1964). (See also UCRL-11531).

37. J. B. Adams, Phys. Rev. 126, 1567 (1962).

38. R. Winston, Phys. Rev. 129, 2766 (1963); R. Winston and V. L. Telegdi, Phys. Rev. Letters 7, 104 (1962);
A. P. Bukhvostov and I. M. Shmushkevich, English trans. Soviet Phys. JETP 14, 1347 (1962).

39. Robert J. Esterling and Norman H. Lipman, Helium Gas Scintillation, Lawrence Radiation Laboratory Report UCRL-11709, October 1964 (unpublished). (Also submitted to Rev. Sci. Instr.).

40. See Fig. 1 of reference 6.

41. A. E. Bjerke, Q. A. Kerns, and T. A. Nunamaker, IRE Trans. Nucl. Sci. N5-9, No. 3, p. 314 (1962).

42. G. Culligan and N. H. Lipman, Rev. Sci. Instr. 31, 1209 (1960).

43. Radiation Instrument Development Laboratory's model 34-12.

44. Figure 2 of reference 6 shows a typical beam spectrum.

45. This circuit was designed by G. Culligan and N. H. Lipman (CERN) and is shown in Fig. 15 of reference 7.

46. R. M. Sternheimer, Rev. Sci. Instr. 25, 1070 (1954).

47. Designed by Mel Brown of the Lawrence Radiation Laboratory.

48. The runs are summarized in Table I of reference 6.

49. J. C. Sens, Phys. Rev. 113, 679 (1959).

50. M. Eckhause, T. A. Filippas, R. B. Sutton, and R. E. Welsh, Phys. Rev. 132, 422 (1963).

51. Neutron multiplicities in the light elements vary from 1.3 in Al to 0.76 in Ca, but, to our knowledge, neutron multiplicities have not been measured accurately in Mg, O, or C.

52. D. J. Hughes and R. B. Schwartz, Neutron Cross Sections (Brookhaven National Laboratory, Upton, N. Y.) BNL-325 (2nd Ed.), 1958.

53. J. D. Seagrave, Phys. Rev. 92, 1222 (1953).

54. M. M. Block, Phys. Rev. 101, 796 (1956).

55. A. M. L. Messiah, Phys. Rev. 87, 639 (1952).

56. A. F. Yano (Long Beach State College), private communication, 1964.

57. H. Morinaga and W. F. Fry, Nuovo Cimento 10, 308 (1953).

58. W. R. Wessel and P. Phillipson, Phys. Rev. Letters 13, 23 (1964).

Table I. Summary of muon-capture rates (in sec^{-1}) in He^3 and He^4.

Authors	$He^3 \rightarrow H^3$	Total He^3	Total He^4	Comments
Experimental				
This experiment	1505±46	2170^{+170}_{-430}	375^{+30}_{-300}	He scintillation
Falomkin et al.[a]	1410±140	2140±180		He diffusion chamber
Edelstein et al.[b]	1450±75			He + Xe scintillation
Bizzarri et al.[c]			363±75	Liquid He bubble chamber
Block et al.[d]			364±46	Liquid He bubble chamber
Anderson et al.[e]			1300	He scintillation, neutron detection
Theoretical				
Primakoff[f]		2500±250	470±70	Closure approximation
Fujii, Yamaguchi[g]	1540±80			"Trion" wave function
Yano[h]	1460	670±30[i]		$g_P = 7 A_\beta$
Goulard, Primakoff[j]		2360±240	324±60	Closure and relativity $g_P = 8 A_\beta$
Fujii, Primakoff[k]	1460±150			
Werntz[l]	1560±80			
Wolfenstein[m]	1400—1500			
Fujii[n]	1660			Hard-core wave function
Duck[o]	1250			Shell-model wave function
Caine, Jones[p]			354±110	Explicit sum over states
Bietti[q]			310	
Bietti, DiPorto[r]			120—220	
Oakes[s]	1500 1410			Irving wave function Irving-Gunn wave function

[a]See reference 8
[b]See reference 9
[c]See reference 10
[d]See reference 11
[e]See reference 12
[f]See reference 13
[g]See reference 14
[h]See reference 4
[i]Breakup rate only
[j]See reference 15
[k]See reference 16
[l]See reference 17
[m]See reference 18
[n]See reference 19
[o]See reference 20
[p]See reference 21
[q]See reference 22
[r]See reference 23
[s]See reference 24

Table II. Corrected numbers of stopping muons (in thousands).

Run	Bμ scaler counts	Sμ scaler counts	-Dead layer Sμ ($2.3 \pm 0.3 \times 10^{-3} \times$ Bμ)	+Decay electron vetos ($5.5 \pm 1.1 \times 10^{-3} \times$ Sμ)	Corrected number of stopped muons
A	56 073	4250 ± 2	129 ± 17	23 ± 5	4144 ± 18
B	65 920	5109 ± 2	152 ± 20	28 ± 6	4985 ± 21
A + B	121 993	9359 ± 3	281 ± 37	51 ± 10	9129 ± 39
LP	116 585	4004 ± 5	268 ± 35	22 ± 5	3758 ± 36
Logic	28 808	2250 ± 2	66 ± 9	12 ± 3	2196 ± 10
B3	25 455	2000 ± 1	59 ± 8	11 ± 2	1952 ± 9
B4	26 167	2000 ± 1	60 ± 8	11 ± 2	1951 ± 9
C	26 463	2000 ± 1	61 ± 8	11 ± 2	1950 ± 9

Table III. He^4 and He^3 breakup events.

1. Run designation	B4	C	B3	A+B	LP	Logic
2. Observed events	1085 ± 45	1080 ± 45	1445 ± 65	5490 ± 130	2460 ± 75	445 ± 25
3. Wall events in observable region	55 ± 40	55 ± 40	30 ± 20	140 ± 100	75 ± 50	33 ± 20
4. Unobserved events	360 ± 90	275 ± 75	1070 ± 540	4200 ± 2100	2280 ± 1200	1650 ± 700
5. Fraction of events not vetoed	1.0	0.95 ± 0.03	1.0	0.824 ± 0.061	0.726 ± 0.085	0.824 ± 0.061
6. Corrected total number of events	1620 ± 130	1590 ± 120	2900 ± 630	13500 ± 3500	7500 ± 1900	3070 ± 1000
7. Corrected number of stopped muons ($\times 10^{-3}$)	1951 ± 9	1950 ± 9	1952 ± 9	9129 ± 39	3758 ± 36	2196 ± 10
8. Breakup events per stopped muon ($\times 10^{3}$)	0.830 ± 0.066	0.816 ± 0.065	1.48 ± 0.33	1.48 ± 0.37	1.99 ± 0.50	1.40 ± 0.46
9. Breakup capture rate (sec^{-1})	378 ± 30	372 ± 30	675 ± 150	675 ± 170	910 ± 230	635 ± 210

Table IV. Triton-recoil events.

1. Run designation	A	B	LP	Logic	B3
2. Counts in triton-recoil peak	11760±400	14030±480	10600±310	5860±270	5290±200
3. Uncertainties contributing to error					
a. Statistical	±110	±120	±100	±77	±73
b. Random background	±125	±180	±100	± 5	±50
c. Electron background	±200	±260	± 60	±200	±100
d. Breakup background	±300	±340	±270	±170	±150
4. Correction factor	1.1760±.0054	1.1760±.0054	1.1853±.0071	1.223±.013	1.1760±.0054
5. Corrected triton-recoil counts	13830±470	16500±570	12570±380	7160±340	6220±240
6. Corrected number of stopped muons (in thousands)	4144±18	4985±21	3758±36	2196±10	1952±9
7. Triton recoils per stopped muon (in thousandths)	3.338	3.310	3.345	3.262	3.187
8. Capture rate (sec^{-1})	1525±53	1512±53	1528±49	1490±72	1456±56

Table V. Triton-recoil-edge correction for different amounts of energy deposited in the gas.

1. Energy left in gas (MeV)	0.77	1.19	1.65	1.90
2. Probability of "seeing" triton recoil(%)	<10	≈50	>90	100
3. Recoil range in helium at 28.9 atm (mm)	0.92	1.29	1.57	1.75±.10
4. Percentage of recoils lost				
(28.9 atm)	0.66	0.93	1.13	
(15.4 atm)	1.22	1.73	2.07	

FIGURE LEGENDS

Fig. 1. Effect on the $He^3 \rightarrow H^3$ capture rate as each coupling coefficient is varied from the values given in Eq. (22). The short dashes show the hyperfine-singlet-capture rate, Λ_s; the long dashes, the triplet-capture rate, Λ_t; the solid line, the total rate, $\Lambda_C = 1/4\,\Lambda_s + 3/4\,\Lambda_t$. The dot in each graph represents the intersection of the measured capture rate and the coupling coefficients of Eq. (22) with uncertainty indicated by the shaded area.

Fig. 2. Dependence of Λ_C, as given by Eqs. (24) and (27), on (a) the vector-coupling coefficient, (b) the axial-vector-coupling coefficient, (c) the induced pseudoscalar coefficient, and (d) the nuclear radius. Each parameter is varied one at a time from the central values given in Eq. (26). The dot in each graph represents the intersection of the measured capture rate and the central value of the parameter with uncertainty indicated by the shaded area.

Fig. 3. Rough diagram of the apparatus showing a simplified schematic of the electronics logic.

Fig. 4. The histograms show the radial variation of muons stopping in a nuclear emulsion. Emulsion A was exposed directly behind the front Lucite window in the target, emulsion B 2-3/4 inches behind the front window, and emulsion C 5 inches behind the window. Each emulsion was exposed to 2×10^6 beam muons. The dashed lines are the muon-stopping distributions, at the same three positions, obtained from the multiple-scattering calculation and are normalized to the same total area as the histograms.

Fig. 5. Pulse-height spectra for each of the major sets of data. (a). Run A, (b). Run B, (c). LP run, (d). Logic run, (e). Run B3, (f). Run B4, (g). Run C, and (h). μ^+He^3 run. The squares are the raw counts in each PHA channel and the dots are the random events calculated for each run.

Fig. 6. Time distribution of μ-e events for 6.75×10^6 Bμ with 6.1 atm of xenon in the target. The dashed lines show the contributions of muons that stop in the various elements of the dead layer. The Mg, O, and Al exponentials were computed from the measured amounts present on the cup-counter wall, and the Xe, C, and randoms were determined by a least-squares fit of the spectrum. The solid line is the least-square fitted sum of the exponentials. Its computed χ^2 per degree of freedom is 1.02.

Fig. 7. Calculated distribution of helium-recoil energies from the elastic scattering of neutrons originating from 1000 muon-capture events in the "dead layer" surrounding the helium gas.

Fig. 8. Effects of the geometry of the gas scintillator on the shape of the deuteron-energy spectrum in the reaction $\mu^- + He^3 \rightarrow d + n + \nu$. A pure phase-space energy distribution was used as input to the Monte Carlo program. The program returned energy distributions for the various running conditions: veto on, veto off, high gas pressure, low pressure. The top scale on the graph indicates the range of the deuterons in the helium gas at high gas pressure (28.9 atm).
——, phase space; --- veto off, HP; — - —, veto on, HP;
— --, veto on, LP.

Fig. 9. Capture events in He^4 (Run B4). The data points are with randoms subtracted and are summed over every five channels. ---, normalized spectrum derived from a phase-space distribution; ——, spectrum derived from Bietti's distribution; ....., the rough effect of varying the counts below ≈ 1.5 MeV by 25%.

Fig. 10. Theoretical deuteron-energy distributions for the reaction $\mu^- + He^3 \rightarrow d + n + \nu$. The solid curve is derived from Yano's spectrum and the dashed from Bietti's. The top scale gives the ranges of a deuteron in helium at 28.9 atm. The shaded area indicates the region masked by the 1.9-MeV triton recoil peak, and the cuts indicate the upper limit of the observed counts for runs B3, A+B, and LP. The dashed lines indicate the estimated upper and lower limits of the deuteron spectrum in the region below ≈ 3 MeV.

Fig. 11. Breakup capture events in He^3 (run B3). The data points are with randoms subtracted and are summed over every five channels. The dashed lines are the normalized spectrum derived from a phase-space distribution; the solid line is the spectrum derived from an average of Yano's and Bietti's distribution; the dotted lines indicate roughly the effect of varying the counts below ≈ 3 MeV by 50%. The other runs with He^3 in the target are similar but have fewer data points.

Fig. 12. The $He^3 \rightarrow H^3$ capture rate with the axial-vector coupling constant and the induced pseudoscalar coupling constant as independent variables. The shaded area indicates the region consistent with the present experiment. The theoretical preferences are indicated by the vertical and horizontal lines. Band I is with $A(q^2)/A(0) = M(q^2)/M(0)$ and band II with $A(q^2)/A(0) = V(q^2)/V(0)$. The width of each vertical band reflects the uncertainty in A(0). The dashed lines are for a V+A weak-interaction theory and for a theory with the weak-magnetism term equal to zero.

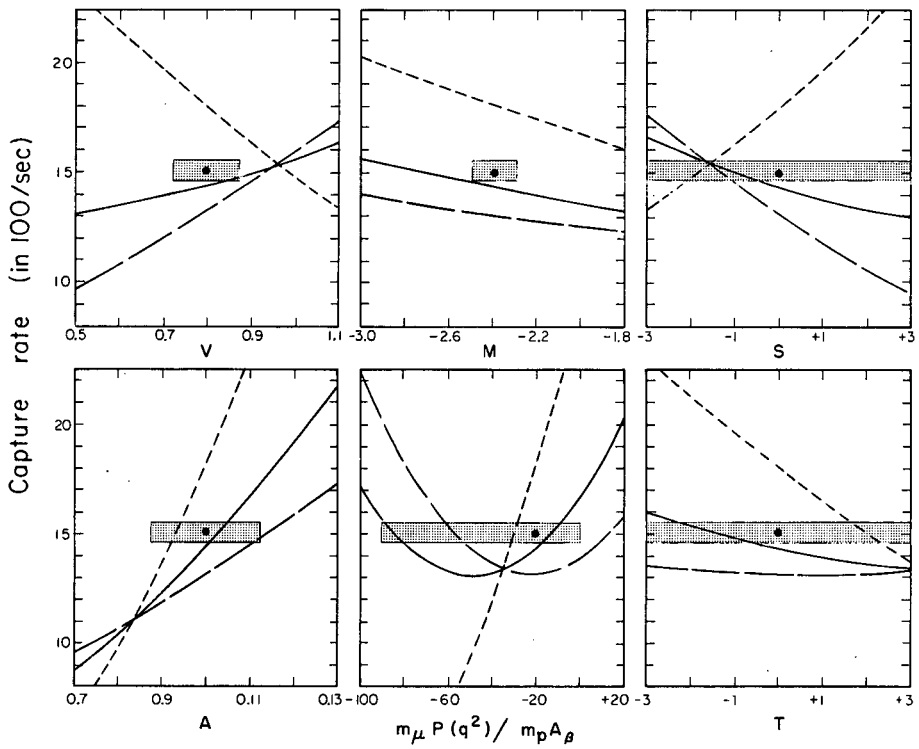
Capture rate (in 100/sec)
20
15
10
0.5
0.7
0.9
1.1
V
-3.0
-2.6
-2.2
-1.8
M
-3
-1
+1
+3
S
0.7
0.9
0.11
0.13
A
-100
-60
-20
+20
$m_\mu P(q^2)/m_p A_\beta$
T
MU-34001

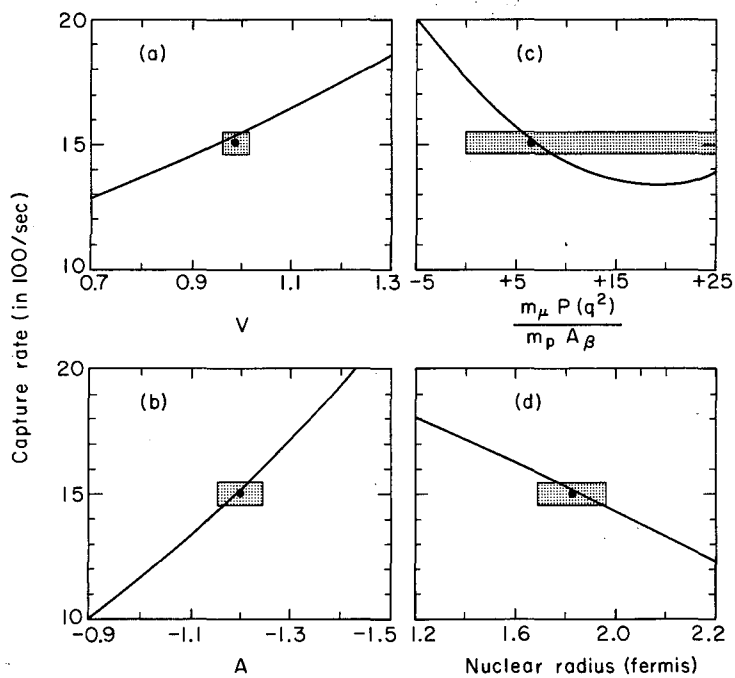
Capture rate (in 100/sec)
20
15
10
(a)
0.7
0.9
1.1
1.3
V
(c)
-5
+5
+15
+25
$\frac{m_\mu P(q^2)}{m_p A_\beta}$
(b)
-0.9
-1.1
-1.3
-1.5
A
(d)
1.2
1.6
2.0
2.2
Nuclear radius (fermis)

MU-34002

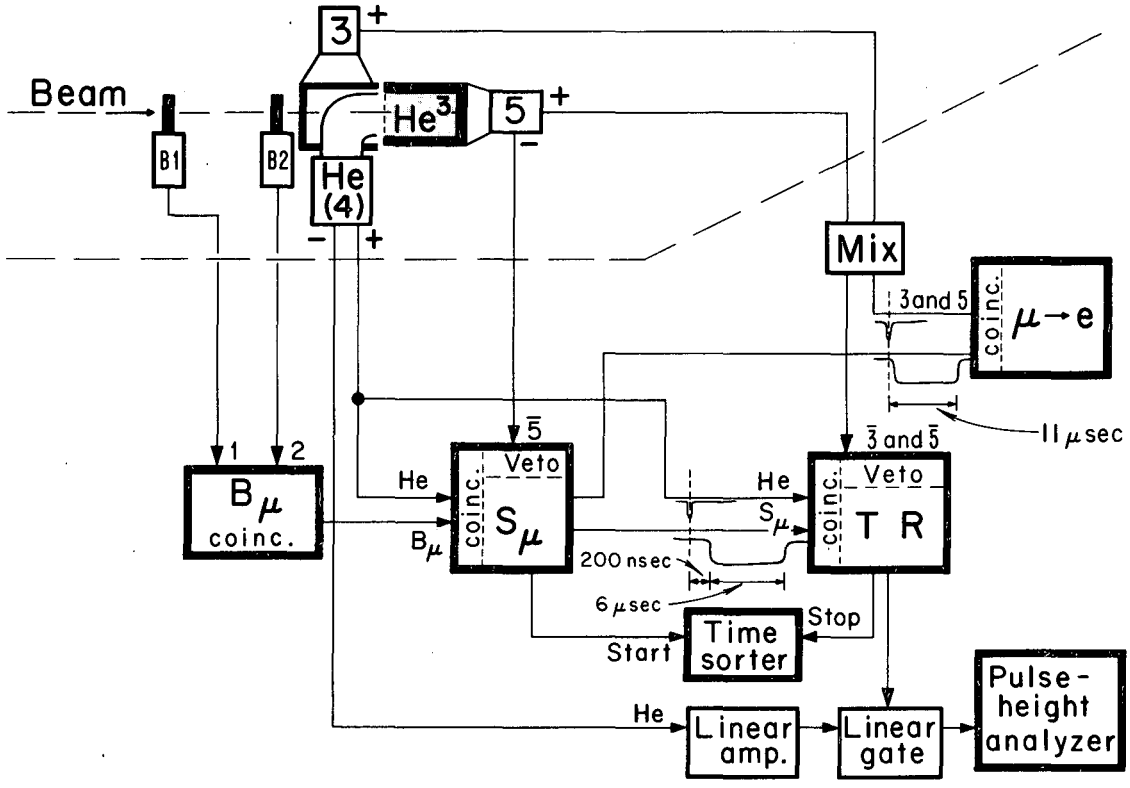
Beam
B1
B2
3
+
He3
5
+
-
He (4)
-
+
Mix
3and 5
coinc.
μ→e
11 μsec
1
2
Bμ
coinc.
He
Bμ
5̄
Veto
coinc.
Sμ
He
Sμ
3̄ and 5̄
Veto
coinc.
T R
200 nsec
6 μsec
Stop
Start
Time sorter
He
Linear amp.
Linear gate
Pulse-height analyzer

MUB-1672

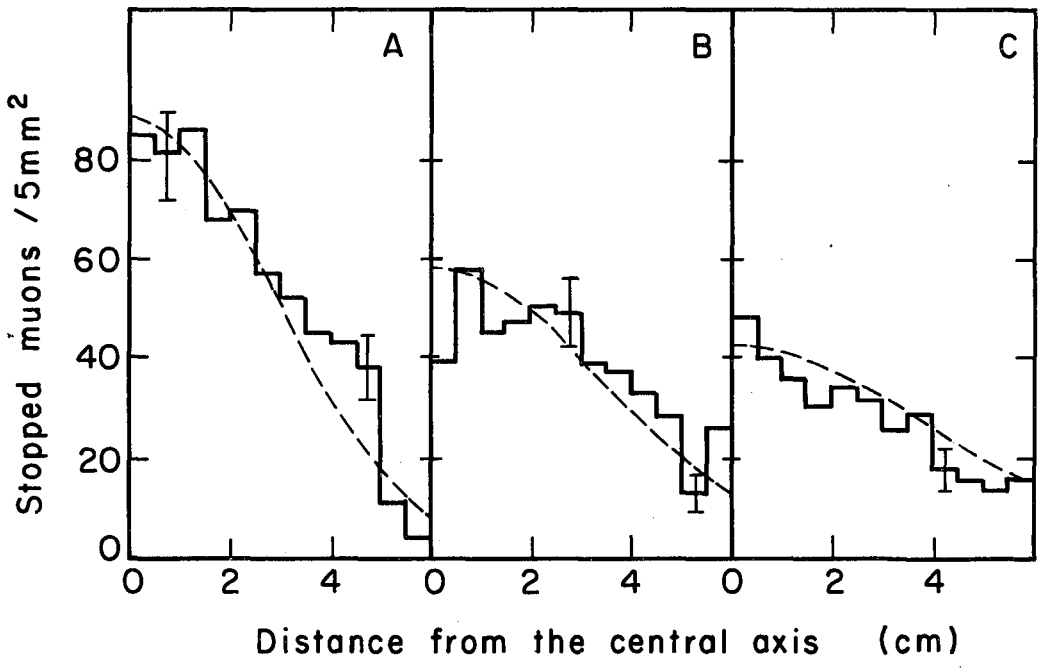
A
B
C
Stopped muons /5mm²
80
60
40
20
0
0
2
4
0
2
4
0
2
4
Distance from the central axis (cm)

MU-33863

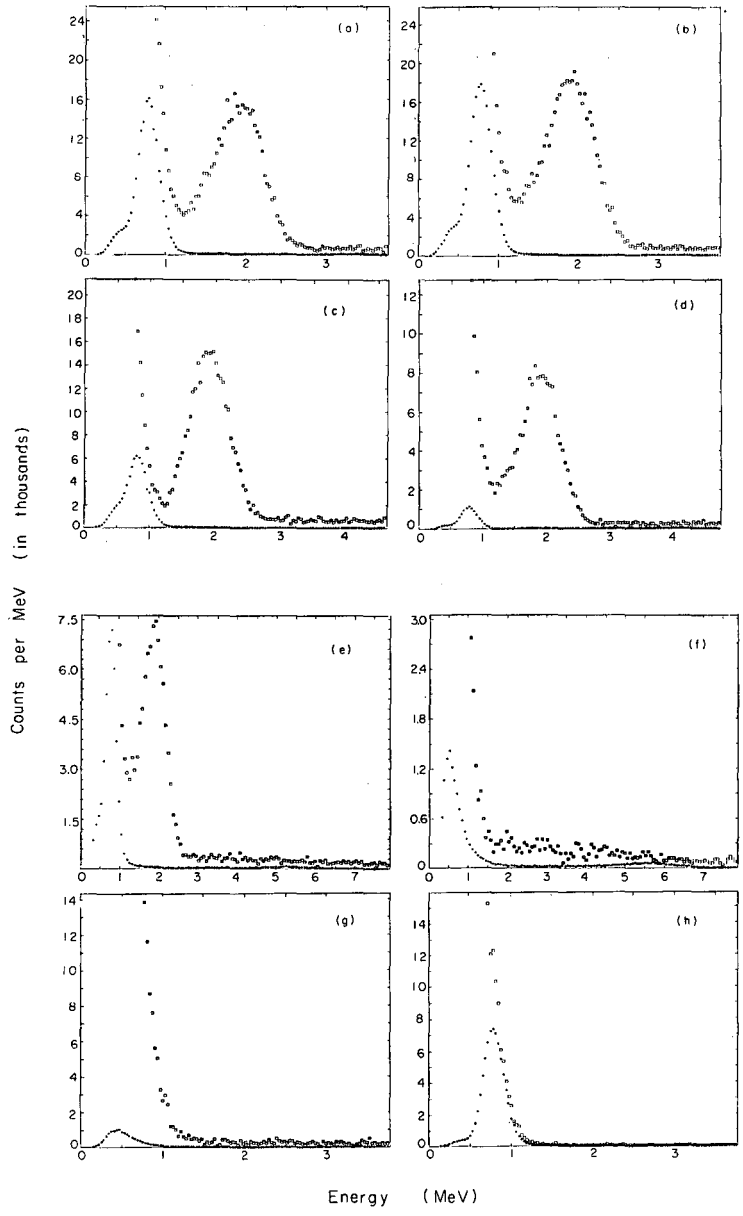

MUB-4319

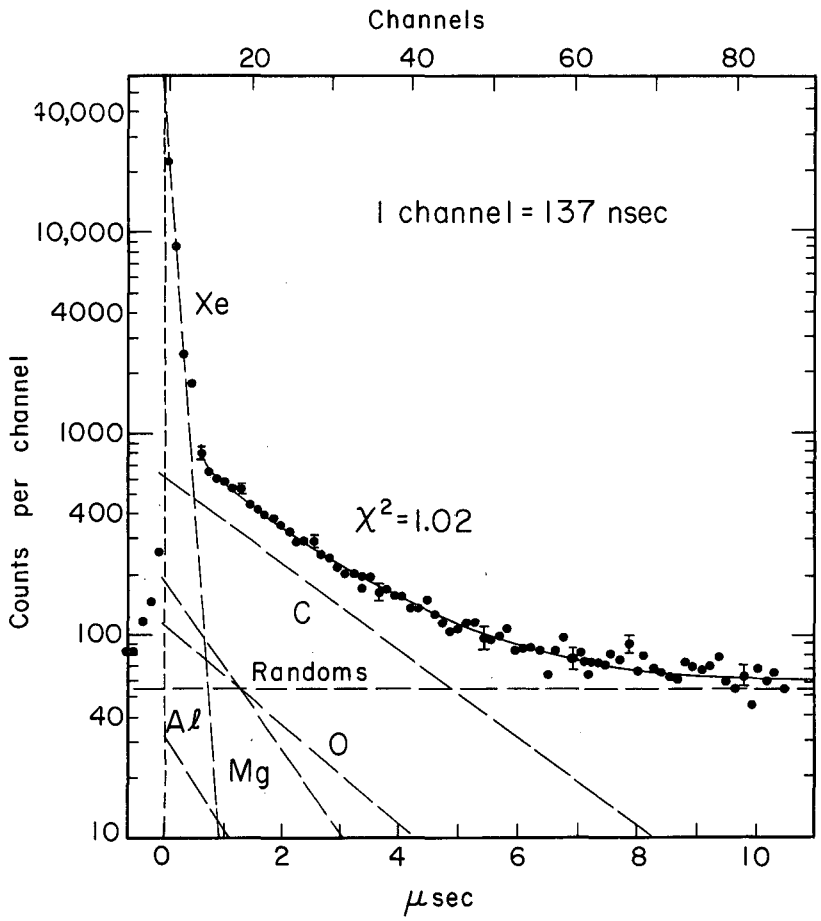
Channels
20
40
60
80
40,000
10,000
4000
1000
400
100
40
10
Counts per channel
1 channel = 137 nsec
Xe
χ^2=1.02
C
Randoms
Aℓ
O
Mg
0
2
4
6
8
10
μsec

MU-33864

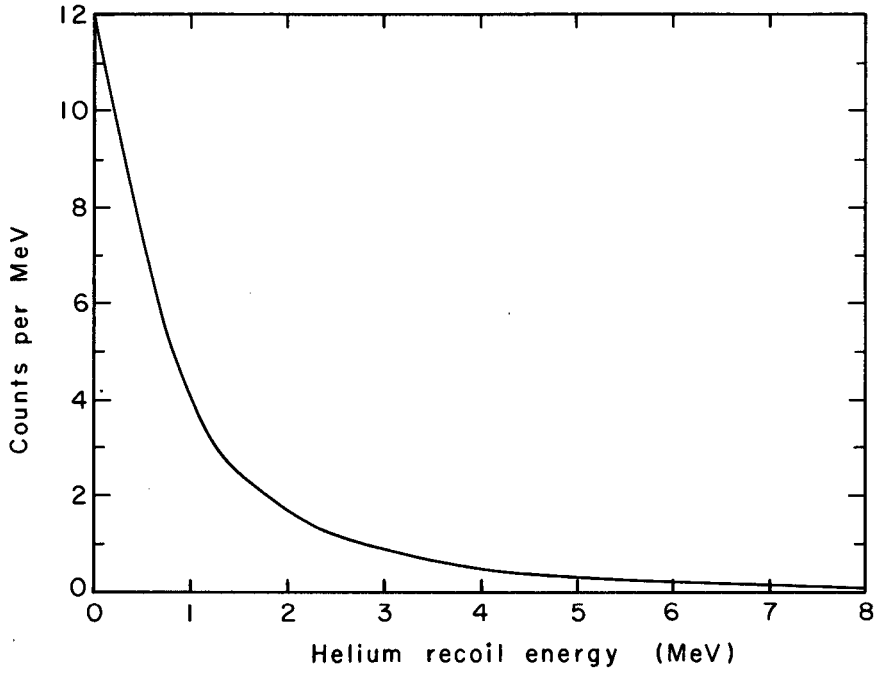
12
10
8
6
4
2
0
Counts per MeV
0
1
2
3
4
5
6
7
8
Helium recoil energy (MeV)

MU-34013

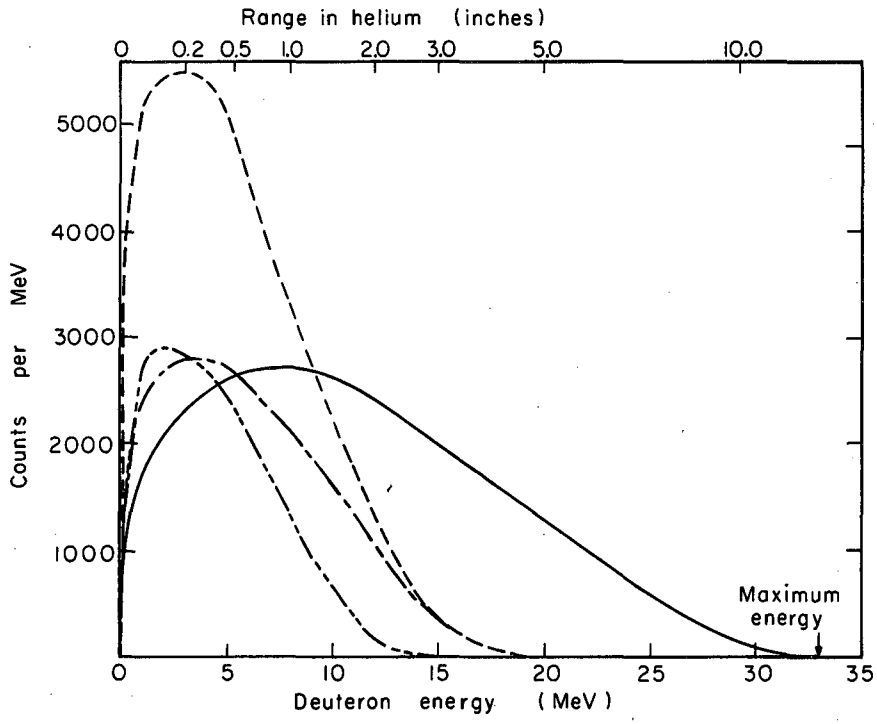
Range in helium (inches)
0
0.2
0.5
1.0
2.0
3.0
5.0
10.0
5000
4000
3000
2000
1000
Counts per MeV
Maximum energy
0
5
10
15
20
25
30
35
Deuteron energy (MeV)

MU-34012

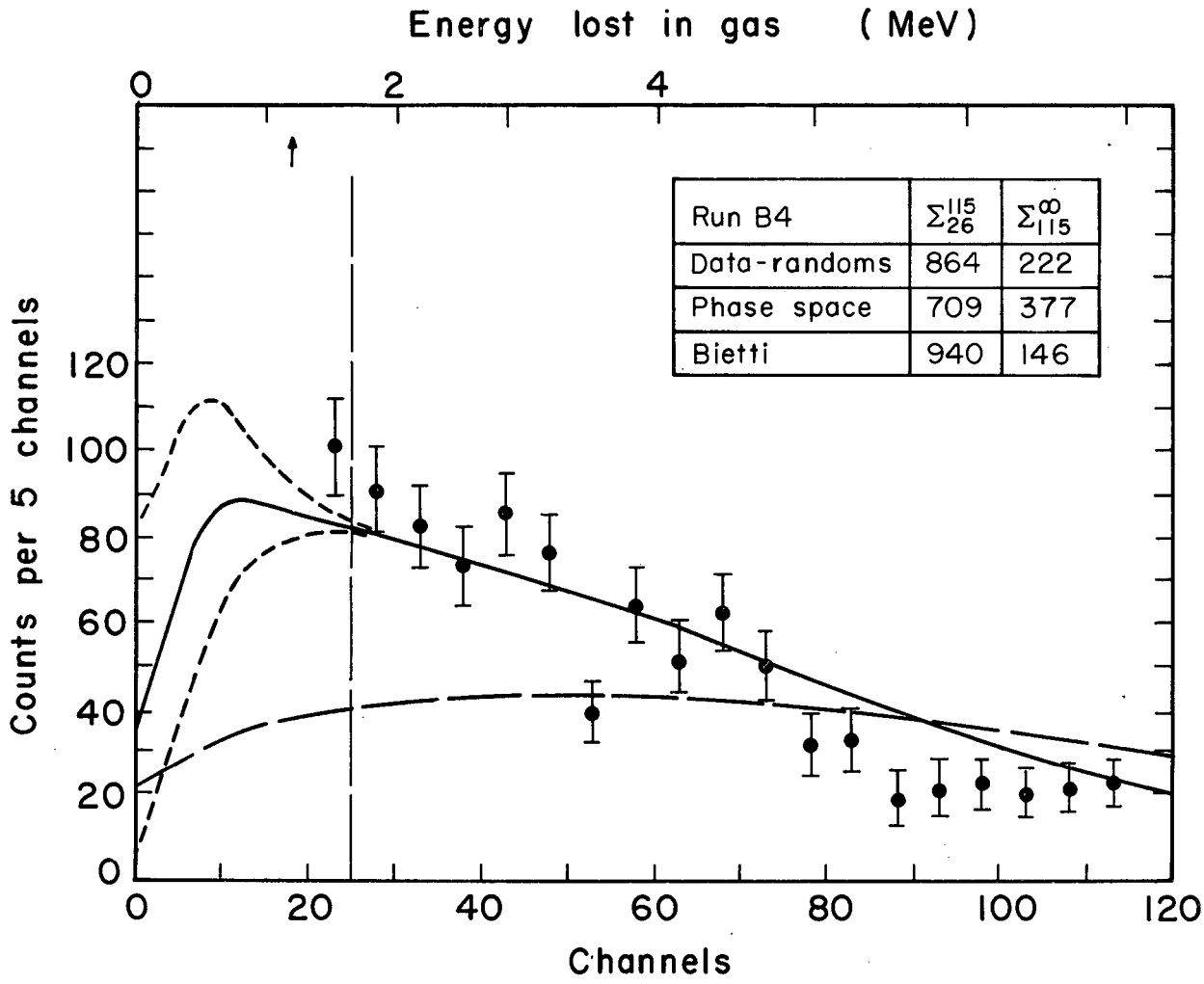
Energy lost in gas (MeV)
0
2
4
Counts per 5 channels
120
100
80
60
40
20
0
0
20
40
60
80
100
120
Channels
Run B4 | Σ_{26}^{115} | Σ_{115}^{∞}
Data-randoms | 864 | 222
Phase space | 709 | 377
Bietti | 940 | 146

MUB-4313

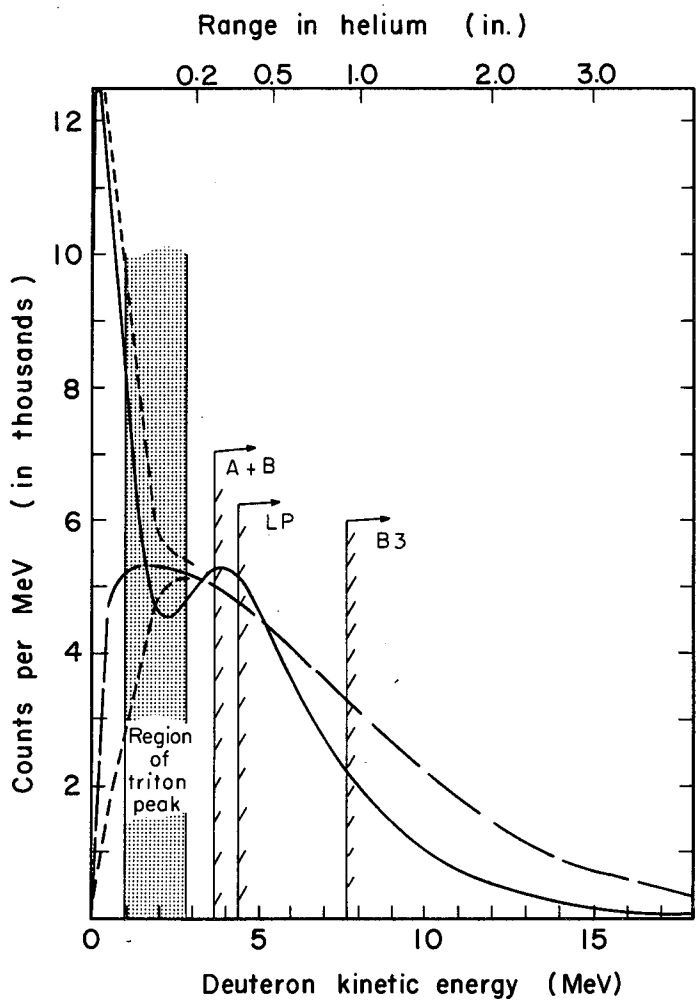
Range in helium (in.)
0.2
0.5
1.0
2.0
3.0
12
10
8
6
4
2
Counts per MeV (in thousands)
A + B
LP
B3
Region of triton peak
0
5
10
15
Deuteron kinetic energy (MeV)

MU-34016

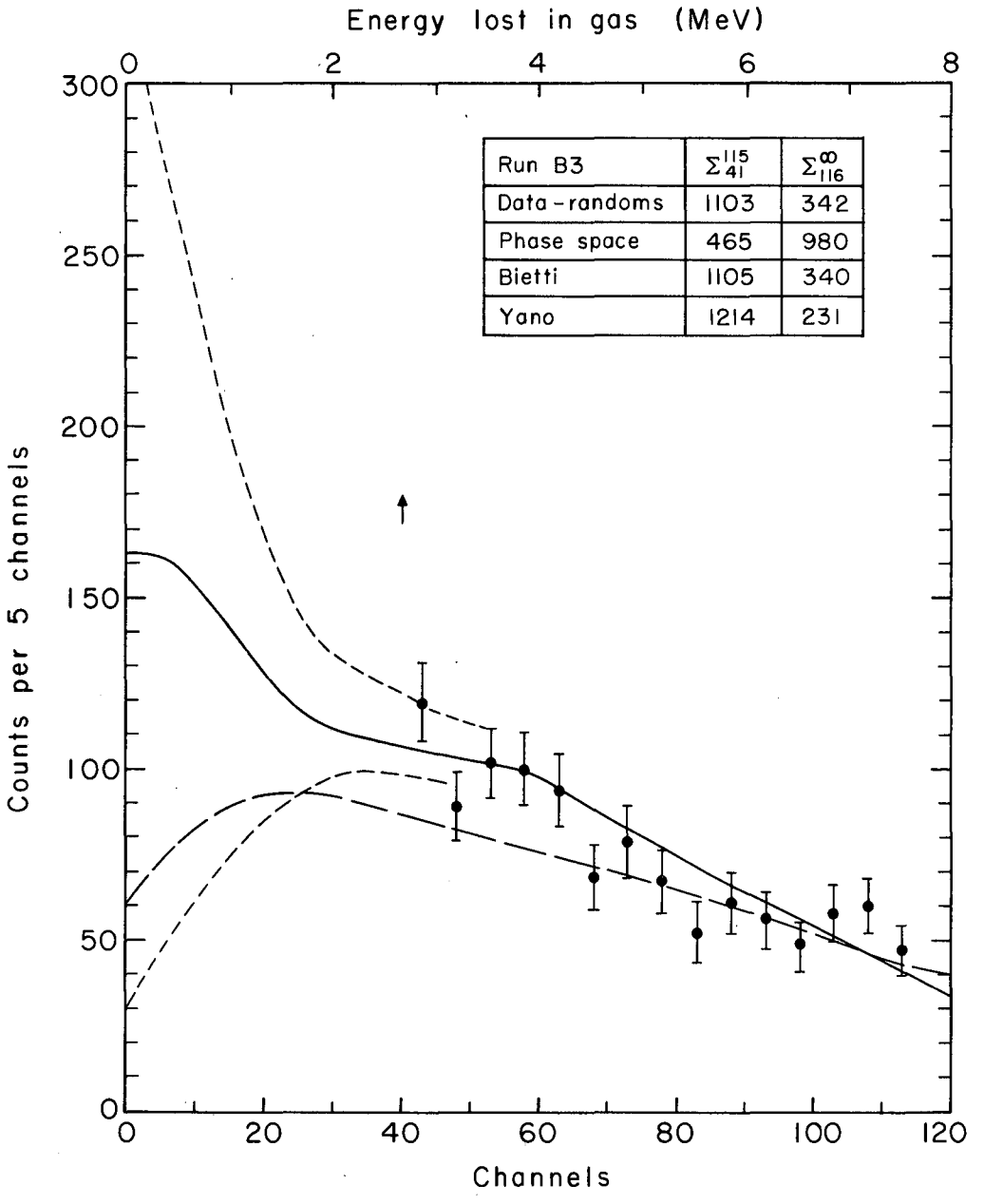
Energy lost in gas (MeV)
0
2
4
6
8
300
250
200
150
100
50
0
Counts per 5 channels
0
20
40
60
80
100
120
Channels
Run B3 | Σ_{41}^{115} | Σ_{116}^{∞}
Data - randoms | 1103 | 342
Phase space | 465 | 980
Bietti | 1105 | 340
Yano | 1214 | 231

MUB-4314

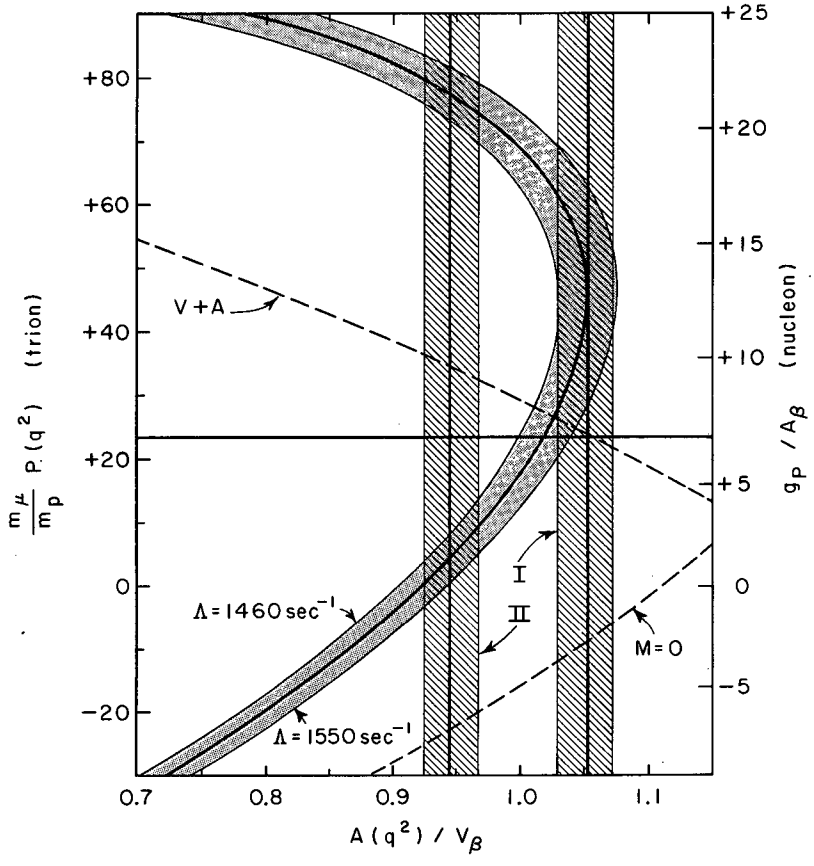
+80
+60
+40
+20
0
−20
+25
+20
+15
+10
+5
0
−5
V+A
Λ=1460 sec⁻¹
Λ=1550 sec⁻¹
I
II
M=0
0.7
0.8
0.9
1.0
1.1
A(q²) / Vβ
mμ/mp P(q²) (trion)
gP / Aβ (nucleon)

MU-34019

This report was prepared as an account of Government sponsored work. Neither the United States, nor the Commission, nor any person acting on behalf of the Commission:

A. Makes any warranty or representation, expressed or implied, with respect to the accuracy, completeness, or usefulness of the information contained in this report, or that the use of any information, apparatus, method, or process disclosed in this report may not infringe privately owned rights; or

B. Assumes any liabilities with respect to the use of, or for damages resulting from the use of any information, apparatus, method, or process disclosed in this report.

As used in the above, "person acting on behalf of the Commission" includes any employee or contractor of the Commission, or employee of such contractor, to the extent that such employee or contractor of the Commission, or employee of such contractor prepares, disseminates, or provides access to, any information pursuant to his employment or contract with the Commission, or his employment with such contractor.